Project No: 603502

DACCIWA

"Dynamics-aerosol-chemistry-cloud interactions in West Africa"

Deliverable

D7.5 Sensitivity and scenario simulations

Due date of deliverable:	31/08/2018
Completion date of deliverable:	31/08/2018
Start date of DACCIWA project:	1st December 2013 **Project duration:** 60 months
Version:	[V1.0]
File name:	[D7.5_Sensitivity_ scenario_simulations_DACCIWA_v1.0.pdf]
Work Package Number:	**7**
Task Number:	**5**
Responsible partner for deliverable:	**ETHZ**
Contributing partners:	**KIT, MO**
Project coordinator name:	Prof. Dr. Peter Knippertz
Project coordinator organisation name:	Karlsruher Institut für Technologie

The DACCIWA Project is funded by the European Union's Seventh Framework Programme for research, technological development and demonstration under grant agreement no 603502.

Dissemination level		
PU	Public	**x**
PP	Restricted to other programme participants (including the Commission Services)	
RE	Restricted to a group specified by the consortium (including the Commission Services)	
CO	Confidential, only for members of the consortium (including the Commission Services)	

Nature of Deliverable		
R	Report	**x**
P	Prototype	
D	Demonstrator	
O	Other	

DOCUMENT INFO

Authors

Author	Beneficiary Short Name	E-Mail
Tanja Stanelle	ETHZ	tanja.stanelle@env.ethz.ch
Katty Huang	ETHZ	katty.huang@env.ethz.ch
Anke Kniffka	KIT	anke.kniffka@kit.edu
Peter Knippertz	KIT	peter.knippertz@kit.edu

Changes with respect to the DoW

Issue	Comments
-	-

Dissemination and uptake

Target group addressed	Project internal / external
Scientic	Internal and external

Document Control

Document version #	Date	Changes Made/Comments
V0.1	25.06.2018	Template with basic structure
V0.2	30.07.2018	1st draft to send to co-authors
V0.3	04.08.2018	2nd draft upload for approval by the general assembly
V1.0	31.08.2018	Final version

Table of Contents

1 Objectives and structure of the report

Atmospheric models have difficulties to simulate the West African Monsoon climate system with its complex meteorological and compositional aspects in an adequate way. Systematic errors are documented in Deliverable 7.4. One objective of this report is to investigate these systematic errors with use of sensitivity experiments performed with different models. One of the identified errors in atmospheric models is the representation of low-level clouds in southern West Africa. Caused by their impact on the radiation, the clouds play an important role in the evolution of the atmospheric boundary layer (Gounou et al., 2012), and the regional climate of West Africa (Knippertz et al., 2011; Hannak et al., 2017). The research group at KIT (Karlsruhe Institute of Technology) performed targeted sensitivity simulations with the ICON model to better understand the role of low-level clouds in the West African Monsoon system. The results are presented in chapter 3.

The research group of the MO (Met Office) contributed to the study of Dearden et al. (2018). They performed large eddy simulations with the Met Office/NERC cloud model (Brown et al., 2015) to simulate low-level clouds over southern West Africa in a lot of detail under idealised conditions. The simulations are constrained and validated using measurements collected during the DACCIWA field campaign in summer 2016. The conclusions and recommendations of that study are embedded into chapter 6 of this deliverable.

Simulating anthropogenic aerosol concentrations and their impact on the climate needs the knowledge of anthropogenic aerosol emissions. Therefore, emission inventories are needed. But the estimated anthropogenic emission fluxes even for present day differ substantially between inventories (see also Deliverable 3.4). The consequences for the simulated climate when applying different emission inventories (including the inventory developed in WP2 of DACCIWA) to model simulations is investigated by the research group of ETHZ (Eidgenössische Technische Hochschule Zürich).

Besides the sensitivity experiments, the realization and discussion of future projections for West Africa is a further task of this deliverable. Until at least the middle of the 21st century the population is expected to increase in West Africa. In particular, the number of inhabitants in cities is expected to grow. Increasing industrialisation is supposed to further result in an increase in anthropogenic emissions. The impacts of these alterations on the West African climate are investigated with the aerosol climate model ECHAM6-HAM2 as well as with the Max Planck Institute Earth System Model (MPI-ESM) coupled to the aerosol module HAM2. The simulations include projected levels of greenhouse gases taken from IPCC inventories. Anthropogenic aerosol emissions are taken from the ACCMIP emission inventory, which were also used in CMIP5 simulations. The group at ETH focuses on the role of the applied Sea Surface Temperature (SST) for the projection of the changing climate in West Africa. They apply SSTs calculated by the CMIP5 simulations of the HadGEM2 and MPI-ESM Earth System models (ESM) to the ECHAM6-HAM2 simulations. Since it is known that ESMs have difficulties to simulate the SST patterns in the equatorial Atlantic correctly, only the simulated changing signal of the ESMs is added to the present day AMIP2 SSTs in additional simulations. Further the impact of the use of a fully coupled Earth System aerosol model or an aerosol climate model with prescribed SSTs for the projected change in climate is investigated. The future projections are presented in chapter 5.

Conclusions of the experiments and the recommendations for model developments, simulation setups, and policy makers are summarized in chapter 6.

2 Model descriptions

2.1 ICON

2.1.1 Operational version at DWD

ICON (Icosahedral Nonhydrostatic, Zängl et al., 2014) is a global numerical weather prediction model recently developed by the Max Planck Institute for Meteorology (MPI-M) and the German Weather Service (DWD). Since January 2015, it is operationally used at the DWD for global predictions. ICON's horizontal grid is based on triangles that cover the globe so that the area of the triangles remains approximately equal everywhere. It is an Arakawa C type grid, which has the distinction of high scalability and easily possible nesting.

Currently, ICON is operated with a global horizontal mesh size of 13 km and 90 vertical levels, with 11 levels up to the first 1000 m (zero topography height). The vertical coordinate is height-based and terrain following in the lower levels but is smoothed in the upper troposphere via the application of a SLEVE coordinate (Leuenberger et al., 2010).

For the dynamical core the continuity equation is formulated in the flux form with density as the prognostic variable in order to achieve mass conservation as close as possible. This enables exact local mass conservation and mass-consistent tracer transport. The equations are solved non-hydrostatically on the global domain. The time integration is performed with a two-time-level predictor–corrector scheme. Apart from the sound wave propagation, this scheme is fully explicit.

ICON has several physical packages that can be chosen. The physics packages that are currently used at DWD are shortly summarized: the fast physics package are inherited from the COSMO model (Doms and Schättler, 2004) but partly reformulated for ICON. The cloud microphysics scheme is the COSMO-EU five-category prognostic scheme (Doms and Schättler, 2004; Seifert, 2008) adapted for ICON with the extension of ice sedimentation. The turbulence scheme by Raschendorfer (2001) solves the prognostic equation for turbulent kinetic energy and for the land-surface interaction TERRA is used in an updated version (Heise, 2006). For the slow developing physics, the Bechtold et al. (2008) convection scheme, the Lott and Miller (1997) subgrid-scale orography scheme and the Orr et al. (2010) non-orographic gravity-wave drag scheme are applied. Radiative transfer is solved with the Rapid Radiation Transfer Model (RRTM) radiation scheme (Mlawer et al., 1997) where a greens function approach is applied for solar bands with approximated diffuse radiation (Barker et al., 2002). The slow-physics parametrizations correspond to the ones from the Integrated Forecasting System (IFS) of the ECMWF.

The results presented in this report were all created from non-ensemble runs. The DWD has ensemble runs for the highly resolved COSMO model in the Germany domain, but global ensemble sets are still under construction. Data assimilation, however, is realized as an ensemble assimilation system for the global runs since January 2016. This is a hybrid combination of an ensemble Kalman filter together with a variation procedure.

2.1.2 Research version from KIT

The research version of KIT corresponds to the ICON operational version but it does not have the data assimilation from DWD. In contrast, it is initialized with analysis fields from ECMWF IFS for each start of a 54 h run. The model was started with a set-up similar to the operational version with the exception of some flags that are specifically useful for tropical environments (e.g. reduction of the moist bias in the lower tropical atmosphere).

2.2 ECHAM6-HAM2

2.2.1 The climate model ECHAM6

ECHAM6 is the sixth generation of the atmospheric general circulation model ECHAM. It is described in detail in Stevens et al. (2013). ECHAM6 employs a spectral transform dynamical core and a flux-form semi-Lagrangian tracer transport algorithm from Lin and Rood (1996). Vertical mixing occurs through turbulent mixing, moist convection (including shallow, deep, and mid-level convection), and momentum transport by gravity waves arising from boundary effects or atmospheric disturbances. Sub-grid scale cloudiness (stratiform clouds) is represented using the scheme of Sundqvist (1989), which calculates diagnostically the grid cell cloud fraction as a function of the relative humidity in the given grid cell once a threshold value is exceeded. Liquid (cloud water) and solid (ice water) condensates are treated prognostically following Lohmann and Roeckner (1996). Radiative transfer in ECHAM6 is represented using the radiation transfer broadband model (RRTMG), which considers 16 and 14 bands for the shortwave (820 to 50000 cm^{-1}) and longwave (10 to 3000 cm^{-1}) parts of the spectrum, respectively (Iacono et al., 2008).

Radiative transfer is computed based on compounds present in the atmosphere and their related optical properties. Trace gas concentrations of long-lived greenhouse gases are specified in the model (except for water vapor). Optical properties of clouds are calculated for each band of the RRTMG scheme using Mie theory and the concentration of liquid water and ice condensates as computed by the 1-moment scheme.

2.2.2 The aerosol climate model ECHAM6-HAM2

The ECHAM6-HAM2 model is a global aerosol climate model. The aerosol module HAM was first implemented in the 5th generation of ECHAM (ECHAM5; Roeckner et al., 2003) by the Max Planck Institute for Meteorology (Stier et al, 2005). Over the past years, the HAM module has been improved and completed with new processes (HAM2) as described in Zhang et al. (2012). The HAM2 module is now coupled to the ECHAM6.

Aerosol microphysics is simulated using the M7 module (Vignati et al., 2004), which accounts for sulphate, black carbon, particulate organic matter, sea salt, and dust. The atmospheric aerosol population is described as a superposition of seven lognormal distributed modes for which standard deviations are prescribed. The total number concentration and masses of the different chemical components are prognostic variables in the model. The modes are divided into soluble, internally mixed modes (containing sulphate) and insoluble, externally mixed modes, which are assigned to different size ranges. The modal diameters can vary and are calculated at each time step from the mass and number concentrations for each mode. Dust particles are considered as part of the soluble and insoluble accumulation and coarse modes. Sedimentation and dry and wet deposition are parameterized as functions of the aerosol size distribution, composition, and mixing state and depend on the ECHAM6 meteorology. The emission fluxes of dust, sea salt, and dimethyl sulfide from the oceans (DMS) are calculated online, based on the model meteorology. Anthropogenic emissions are prescribed.

The optical properties of the modelled aerosol concentrations are employed in the radiative transfer calculations. The aerosol activation and ice nucleation parameterizations of the two-moment stratiform cloud scheme of Lohmann et al. (2007) provide links between the simulated aerosol population and the number concentrations of cloud droplet and ice crystal. So the model accounts for aerosol effects on cloud microphysics (droplet number and size) and macrophysics (liquid water path).

All ECHAM-HAM simulations shown in this Deliverable are conducted with the ECHAM6.3-HAM2.3 model version. They were performed with a T63L47 resolution (approx. 200 km x 200 km horizontal resolution). The details of the simulation setup will be discussed in the respective chapters.

2.2.3 MPI-ESM-HAM2

MPI-ESM-HAM is the earth-system model version of the ECHAM6-HAM2 model, where the atmospheric aerosol-climate model is coupled to an ocean model and carbon cycling between the various earth system components is considered. Aside from the atmospheric component ECHAM6-HAM2 as described above, additional components of the model include the ocean-sea ice model MPIOM (Marsland et al. 2003, Jungclaus et al. 2013) and the ocean biogeochemistry sub-model HAMOCC (Ilyina et al. 2013). Contrary to the standard ECHAM6-HAM2 distribution, the atmospheric model included in the version of MPI-ESM-HAM used in the current study additionally considered the presence of organic aerosols from marine origin, which can further act as ice nucleating particles for the initiation of ice crystals in clouds. The ice nucleation parametrization also differs from the standard version, which follows Lohmann and Diehl (2006), and follows instead Ickes et al. (2017) for immersion freezing of dust and Huang et al. (2017) for that of marine organic aerosol.

3 Role of low-level clouds in the West African monsoon system

The complex multi-scale West African monsoon (WAM) system is currently not adequately represented in climate and weather models. One potential reason are the extensive ultra-low stratus clouds that form during night time in southern West Africa (8°W–8°E, 5–10°N) in connection with the nocturnal low-level jet (NLLJ). Since these clouds often persist until midday, they have a strong impact on the local radiation budget, hence influence the boundary layer development. At their maximum diurnal extent, they cover a vast area of about 850,000 km^2. Their formation is linked to cold advection and turbulent mixing associated with the NLLJ and radiative cooling (Schrage and Fink, 2012; Schuster et al., 2013; Kalthoff et al., 2018). A recent study based on climate models participating in CMIP5 and the Years of Tropical Convection (YoTC) project indicates that the majority of models are incapable to reproduce the lifecycle of these low clouds (Hannak et al. 2017). Therefore, the impact of the radiative effects of these clouds on the larger WAM system and its diurnal cycle was analysed.

The influence of low-level clouds on the development of the regional-scale dynamics in southern West Africa is assessed via sensitivity simulations with the numerical weather prediction (NWP) model ICON of the German Weather Service. For these simulations, the optical thickness of the cloud decks below 700 hPa in the region 5 – 10° N and 8W – 8E (in the following referred to as “DACCIWA box”) is multiplied by an opacity factor f_{op} prior to calling ICON's radiation scheme. After the computations of the radiation scheme the field is set back to the original values. This way, the radiative effects of the clouds on the further development of the model's atmosphere can be analysed in a fully nonlinear fashion. The experiments cover the monsoon season July 2006, with standard as well as convection-permitting simulations. The simulations are initialized with European Centre for Medium-Range Weather Forecasts (ECMWF) ERA-Interim re-analysis and include 5-day runs started every 4 days for the sensitivity experiments in standard and convection-permitting configurations. Another set of 10 day runs was produced for which the application of the opacity factor was switched-off after 4 days in order to test the temporal stability of the induced changes. We used ICON's nesting capability to obtain grid-spacings of 13.2 km (standard run) and 6.6 km (convection-permitting) over the region of interest. The sets were evaluated with respect to a) their sensitivity to the opacity of low clouds and b) the differences in diurnal cycles resulting from the treatment of convection. The set with explicit convection is called EXPL hereafter, and the parametrised one was named PARAM.

Comparisons with ground and satellite-based observations of rainfall and radiation show substantial deviations between the two model configurations and with the observations. PARAM reproduces the coastal rainfall maximum over the Niger Delta but cannot adequately create the inland penetration of precipitation. PARAM results in realistic surface solar irradiance (SSI) but has too much extinction

of shortwave radiation in the atmosphere. This causes a negative bias in outgoing shortwave radiation (OSR). The case EXPL is also capable of reproducing the coastal rainfall but it has a much too strong Sahelian rainband, which is also displaced farther north than observed. EXPL also shows reduced SSI and enhanced OSR compared to satellite measurements caused mainly by low-level clouds. PARAM generally tends to have substantially more high and less low clouds compared to EXPL. This demonstrates the enormous influence of convective parametrisation on the West African meteorology as already documented in Marsham et al. (2013). Both model versions show a noticeable disagreement with measurements. Nevertheless, they can be used for the sensitivity analysis in terms of process analysis and robustness of the found sensitivity, but most likely not for quantitative analysis.

Making low clouds more transparent to short- and longwave radiation creates a complicated atmospheric response, as will be discussed in the following. Nevertheless, this response depends monotonically on the opacity factor f_{op} as can be seen in Fig. 3.1. Here, the response of the atmospheric system depending on f_{op} is depicted with monthly mean box-averages of temperature and precipitation plus surface and top of atmosphere radiative quantities. The original field is marked with f_{op} = 1.0. Averages are presented for EXPL and PARAM in cyan or blue, respectively. All variables show a logarithmic dependence on f_{op}. OSR and longwave surface radiation (SLI), temperature and pressure decrease with increasing opacity of the low-level clouds, while the outgoing shortwave and longwave radiation components OSR and OLR increase.

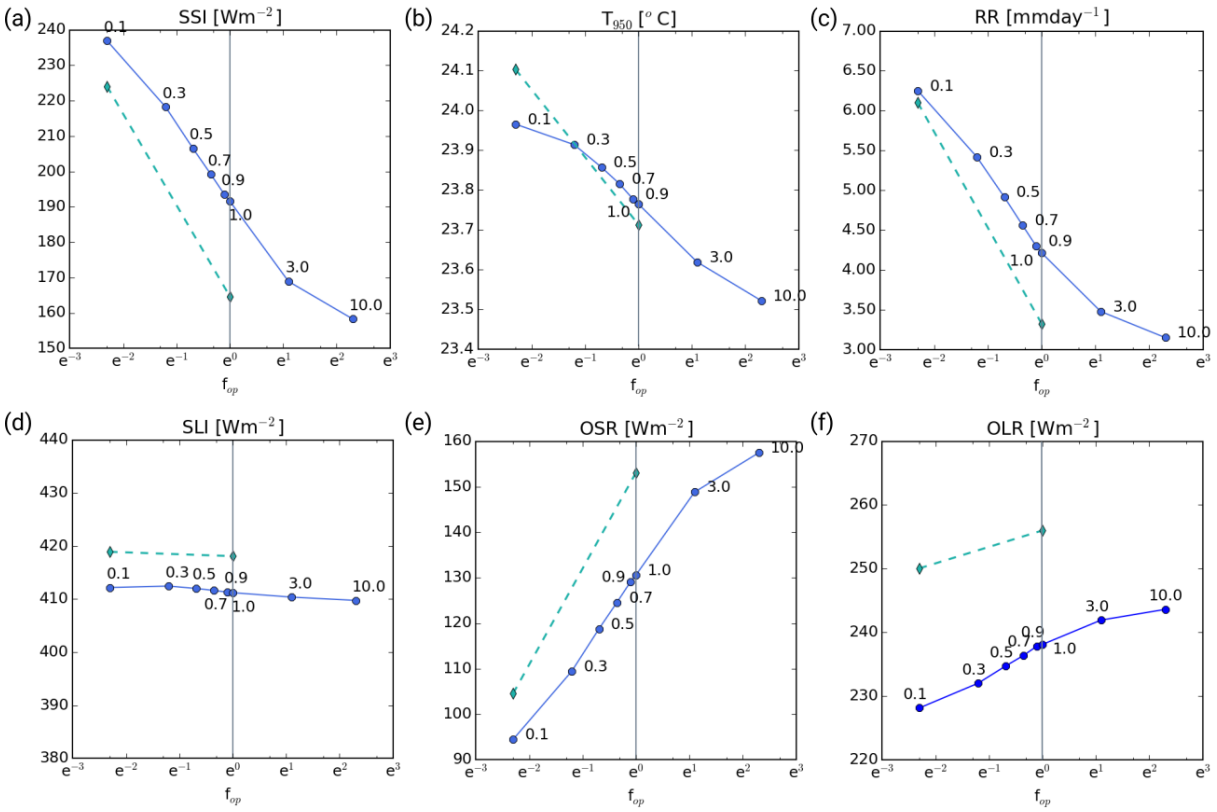

Figure 3.1: **SSI (a), T_{sfc} (b), RR (c), SLI (d), OSR (e) and OLR (f) depending on the opacity factor f_{op}, July 2006, DACCIWA box average, plotted with logarithmic scale on the x-axis. The experiment PARAM with 13.2 km horizontal resolution is depicted with the solid blue line, while the dashed cyan line denotes the experiment EXPL with explicit convection and 6.6 km horizontal resolution, compare Table 1. The thin grey line marks the position of the control run f_{op} = 1.0 (figure taken from Kniffka et al. (subm.)).**

The main effects are illustrated in more details in Fig. 3.2 in a schematic overview for the case EXPL that has a more realistic diurnal boundary layer development than PARAM. In this figure, mainly the

daily mean effects are depicted, but for some parameters the diurnal evolution will be discussed, too. Note that in the NWP simulations SSTs stay largely constant during the short run time. The southern and northern borders of the box with cloud modifications, i.e. 5 and 10°N, are marked by vertical lines in Fig. 3.2.

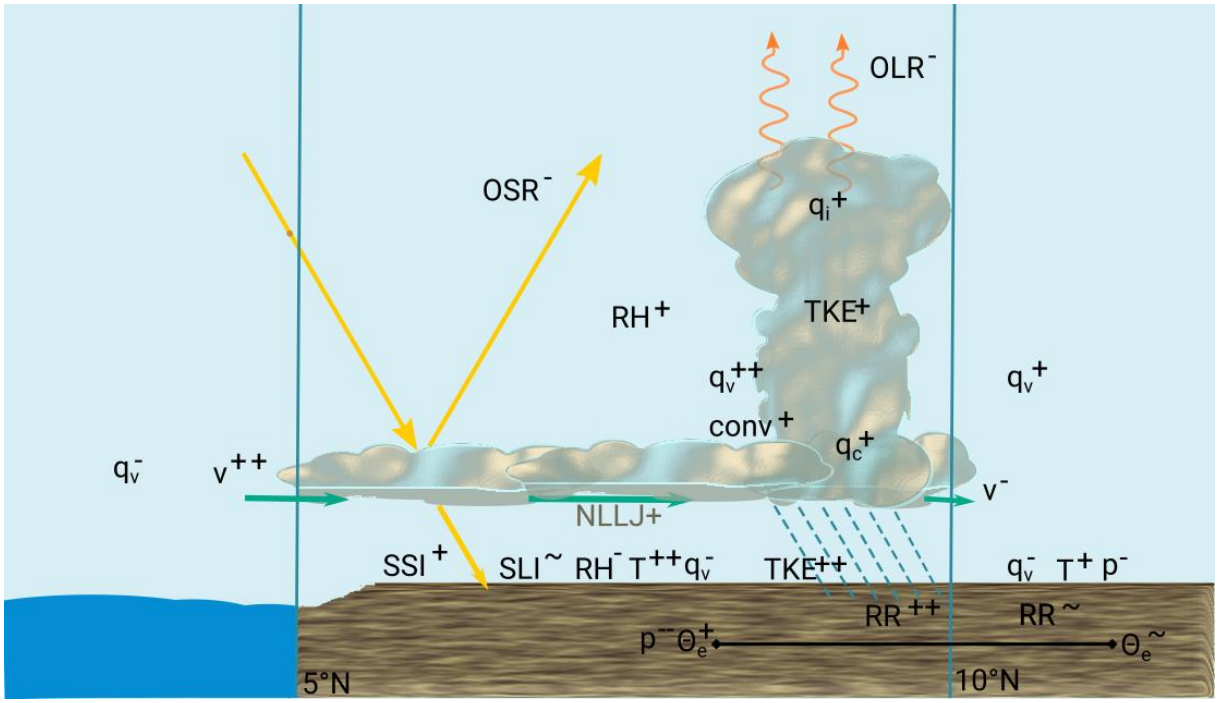

Figure 3.2: Conceptual sketch of the process chain when changing optical properties of low clouds (figure taken from Kniffka et al. (subm.)).

The first and most obvious aspect is that more transparent low clouds lead to more solar radiation reaching the ground (SSI+) and less being reflected to space (OSR–) during daytime, compare Fig. 3.1. Therewith an increase in low-level temperatures arises (see Fig. 3.1), particularly in the afternoon (T++). This causes a decrease in stability and triggers more turbulent mixing (TKE++) and more deep convection (conv+), which leads to more convective mixing and a substantial increase in precipitation (RR++). At maximum the monthly average rainfall increases by a factor of 5, on average over the complete box by a factor of 2 (compare Fig. 3.1). The more or less logarithmic dependence of rainfall on the opacity factor (f_{op}) indicates the strong and dominating control of the low clouds on the triggering of convection. Additionally, the low-level heating and free-tropospheric increase in latent head causes a noticeable decrease in surface pressure, mainly around 18 UTC (coinciding with the convective peak, p--). With that, the gradient to the south is sharpened which brings about an enhancement of the nocturnal low-level jet (NLLJ+) and a stronger inflow from the Atlantic (v++). At the same time, the export to the Sahel is reduced (v-). Therewith the meridional convergence is enhanced and more moisture can concentrate over southern West Africa. With the enhanced turbulence and convection, the additional moisture can be transported upwards (qv++). Since this effect dominates over temperature, relative humidity (RH+), cloud water (qc+) and cloud ice (qi+) increase in the troposphere. Only very close to the surface and during daytime, the enhanced advection of dry air from the ocean (dry because of the colder temperatures and therefore less moisture uptake capability, plus more subsiding motions) and the deeper PBL due to intensified mixing lead to a qv and RH decrease (qv- and RH-). At 18 UTC, this also leads to less low-level cloud cover and cloud water (not shown). On all other times of day, the cloud cover and water content are increased due to the available moisture. This is indicative of a negative feedback mechanism of low clouds. The high-cloud cover and cloud ice content increase too, which is reflected in the slightly

reduced outgoing longwave radiation (OLR-). Surface effects of longwave radiation are small (SLI-) since the atmosphere already contained a large amount of water vapour and clouds (Fig. 3.1). The latter is a strong indication of dynamic adjustments in the model. A recent study by Hill et al. (2018) (also part of DACCIWA) estimated the effect of low clouds over southern West Africa from pure radiative transfer simulations on satellite-derived cloud data. While for the shortwave component (i.e. SSI and OSR) both approaches point in the same direction, the longwave components are reversed.

The regional impact outside of the modified box is much smaller, though it can be observed that the signals produced in the box travel northwards at night. Over the ocean the most significant change is a free tropospheric drying that can be caused by enhanced subsidence related to the increase of convection over adjacent land. North of the box over the Sahel, approximately downstream, low-level advection with the southerly monsoon flow shows the largest effects. The impact of the modification in the box can be observed up to 20°N (T+ and p-). Moisture on the other hand, is advected in the low levels with the mean flow, but since there is an excess daytime drying in the lowest levels of the box (qv-), the northern regions receive a drying, too that is transported with a pulsing signature. Above that, slight moistening can be found due to advection of the moist air with the deep monsoon flow from the DACCIWA column towards the Sahel (qv+). For all those reasons, the impact of the modifications on monthly average rainfall outside of the DACCIWA box is fairly small, apart from the immediate vicinity of the box (RR~). However, all the observed changes can still lead to variations in the development of the diurnal cycle of convection and the organisation of mesoscale convective systems. In our study such effects can be seen indeed, but due to the chaotic nature of the dynamics in the Sahel, a much longer time-series would be needed to put a statistical analysis on more solid grounds.

We analysed the impact on the larger scale monsoon flow by using the concept of Eltahir and Gong (1996). In this concept, the monsoon flow can be described as a direct thermal circulation for moist atmospheres (Zheng et al., 1999; Hurley and Boos, 2013). Here, the gradient of a single atmospheric state variable, namely the equivalent potential temperature (θ_e), can be used to describe the strength of the monsoon flow. Due to the compensating effects of temperature and moisture changes over the Sahel, only small changes in θ_e can be observed. Note, that substantial changes in θ_e occurred in the DACCIWA box. Since the maximum of θ_e is located in the Sahel and the minimum over the ocean, only small changes in the total gradient of low-level θ_e occurred. For this reason, errors or changes in low-level clouds over southern West Africa will likely have substantial local impacts but the downstream regions are not too much affected, at least not in terms of rainfall.

As a last point, we would like to sum up the comparison between EXPL and PARAM. The impacts of our sensitivity experiment on the averages of the atmospheric state variables such as temperature and radiative quantities are the same (compare Fig. 3.1). However, substantial changes can be seen in the diurnal evolution of the PBL and free troposphere. Due to the parametrisation of convection, PARAM's diurnal cycle in rainfall is shifted forward by about 3 hours as is often observed with this kind of parametrisation (Marsham et al., 2013). Therefore, the sensitivity with respect to the low clouds is influenced. The surface heating effects are not as strong as in EXPL and pressure and wind signals are reduced, too. Vertical mixing is small and has a different timing, which impacts the diurnal cycle of the vertical distribution of moisture. At midday, the differences between PARAM and EXPL are most pronounced. PARAM shows a significant low-level increase of moisture (with transparent low clouds) related to the enhanced convective rainfall, while EXPL shows the opposite due to stronger dry advection and vertical mixing. Overall, a decrease of low clouds and cloud water can be stated in PARAM while there is an increase in EXPL at most times of day. The behaviour of PARAM could serve as an explanation, why many models with convective parametrisation possess large negative biases in low-level cloud cover (Knippertz et al., 2011; Hannak et al., 2017). The

export of differences in temperature and moisture as described above for EXPL are somewhat reduced for PARAM and also have a different timing.

To sum up, our findings suggest, that the low-cloud errors often present in climate models (Hannak et al., 2017) can explain the large precipitation errors in the Guinea Coastal region, but not in the Sahel when considering only the average amount of rainfall. The experiments are not only a sensitivity study but were designed to mimic the effects of variations in aerosol. Similar effects can be expected from changes in low-level aerosol, as already documented in a case study by Deetz et al. (2018a). To be more precise, increases in aerosol content (and cloud optical thickness) would lead to a reduction of SSI. This would likely reduce precipitation in the respective region as suggested by our cloud studies. Such increases in anthropogenic activity have been observed and are projected to increase given the overall dynamic population and economic development (see Knippertz et al., 2015). In this study, the clouds were manipulated directly, since the focus was put on the clouds themselves and errors in the microphysical schemes were excluded in this way, but it would be desirable to conduct studies with realistic changes in aerosol loading and treatment of aerosol processes together with microphysical cloud formation. A suppression of rainfall by aerosols for example could create a positive feedback by reducing wet removal. Future work should also investigate longer-term effects of the misrepresentation of low clouds in climate models, e.g. moderated through effects on rainfall, soil moisture and evaporation.

4 The West African Monsoon system simulated by ECHAM6-HAM2

4.1 Performed simulations

A part of the simulations was already presented in Deliverable 7.4. A comprehensive model evaluation is given there. Here we will not repeat this work but focus on the implication of the used aerosol emission inventory on the representation of the climate in southern West Africa. In all simulations, AMIP2 SST and SIC are applied. The simulations differ only in the applied aerosol emission inventories. Anthropogenic and biomass burning emissions are prescribed by (1) the ACCMIP (Atmospheric Chemistry and Climate Model Intercomparison Project) emission inventory (Lamarque et al., 2010), (2) ACCMIP + GFAS (Global Fire Assimilation System; Heil et al., 2010) for biomass burning, (3) the HTAPv2.0 emission inventory + GFAS, (4) the Community Emissions Data System (CEDS, http://www.globalchange.umd.edu/ceds) , and (5) the emission inventory developed during the DACCIWA project (WP2, Deliverable 2.1) for Africa and ACCMIP elsewhere. Seasalt and dust emission fluxes are calculated online in dependency of meteorological fields provided by the atmospheric model. The aerosols modify the climate via the direct and indirect aerosol effects. The performed simulations are summarized in table 4.1.

Table 4.1.: Performed simulations. GFAS biomass burning emission fluxes are multiplied by a factor of 3.4 as recommended by Kaiser et al (2012).

	Anthropogenic emissions	**Biomass burning emissions**
accmip	ACCMIP (Lamarque et al., 2010)	ACCMIP (Lamarque et al., 2010)
accmip_gfas	ACCMIP (Lamarque et al., 2010)	GFAS (Heil et al., 2010)
htap	HTAP (http://edgar.jrc.ec.europa.eu/htap_v2/)	GFAS (Heil et al., 2010)
ceds	CEDS (http://www.globalchange.umd.edu/ceds/)	GFAS (Heil et al., 2010)
dacciwa	DACCIWA (WP2, deliverable 2.1)	GFAS (Heil et al., 2010)

As seen in Figure 4.1, the emission inventories show substantial differences. The annual cycle is given by the biomass burning emissions, the anthropogenic fluxes do not show monthly variations. This explains the low emission fluxes in simulation “accmip” during winter. This is the only simulation where we did not apply the gfas biomass burning emission inventory (Table 4.1). In general, the

main difference between the accmip and gfas biomass burning emissions are caused by the application of the recommended factor of 3.4 by Kaiser et al. (2012). At the Guinea Coast the biomass burning emission occur during winter. But during summer a large contribution of biomass burning aerosols is transported to the Guinea Coast from their source region in Central Africa.

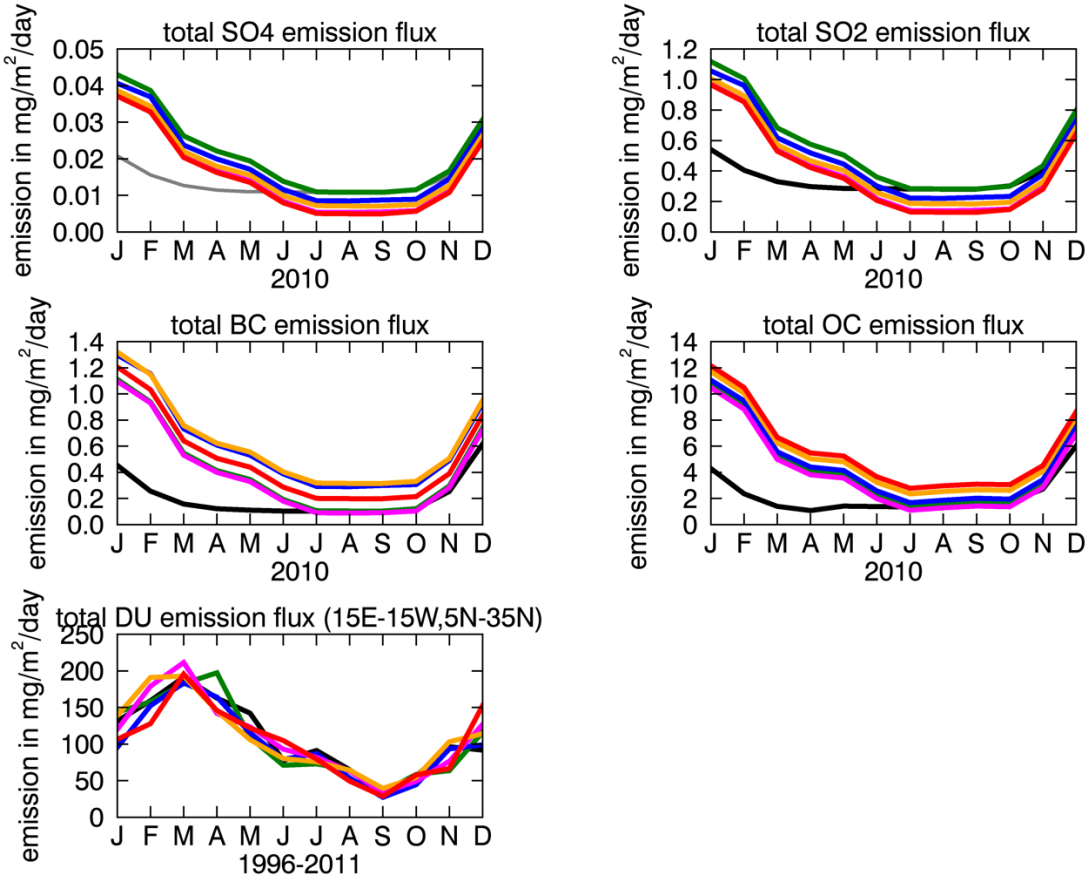

Figure 4.1: Mean aerosol emission fluxes (black: accmip; green: accmip + gfas; orange: ceds; blue: htap, red: dacciwa). The anthropogenic emission fluxes are averaged over a domain of 5° N – 15° N, 15° W – 15° E. The dust emission fluxes are averaged over a domain 5° N – 35° N, 15° E – 15°W.

4.2 Aerosol concentrations

A comparison between the ECHAM6.3-HAM2.3 simulated aerosol distribution and observations is already reported in deliverable 3.2. For this comparison we performed a simulation where the large-scale meteorology was nudged to ERAinterim. The accmip emission inventory was applied for both, anthropogenic and biomass burning emissions. It is found that the model was able to reproduce the biomass burning plume in the south-east of the DACCIWA region. But it failed representing the AOD plume in South-East Niger. The simulated AOD is in general agreement with observations in the Guinean coastal region as well as in Sahelian stations, but the AOD is slightly underestimated there.

During winter time the regional aerosol content is dominated by mineral dust particles which are emitted in the Sahara and transported with the Harmattan winds into southern West Africa. There are variations in dust concentrations between the simulations. Dust emissions are calculated online in dependency of the vegetation cover, wind speed, and soil properties. The changes in the emission fluxes are caused by induced changes in wind speed due to feedbacks between aerosols, radiation, and clouds.

In DACCIWA, we focus on summertime. In the boundary layer, anthropogenic plus biomass burning aerosol concentrations are on the same order of magnitude as the dust concentrations during summer (figure 4.2). In July the simulations with the highest aerosol burden in the boundary layer is “dacciwa”. The lowest surface aerosol concentration is simulated in “accmip-gfas”. This is very surprising because the biomass burning emissions prescribed in simulation “accmip-gfas” are three times larger than the ones in “accmip”. But due to feedback mechanisms the dust concentration is higher in “accmip”. This points out the important need to understand the dust emission – transport – deposition processes to simulate the aerosol distribution in southwest Africa correctly.

But south of the “dacciwa box”, the aerosol burden is highest in simulations where gfas biomass burning emissions are applied (figure 4.3).

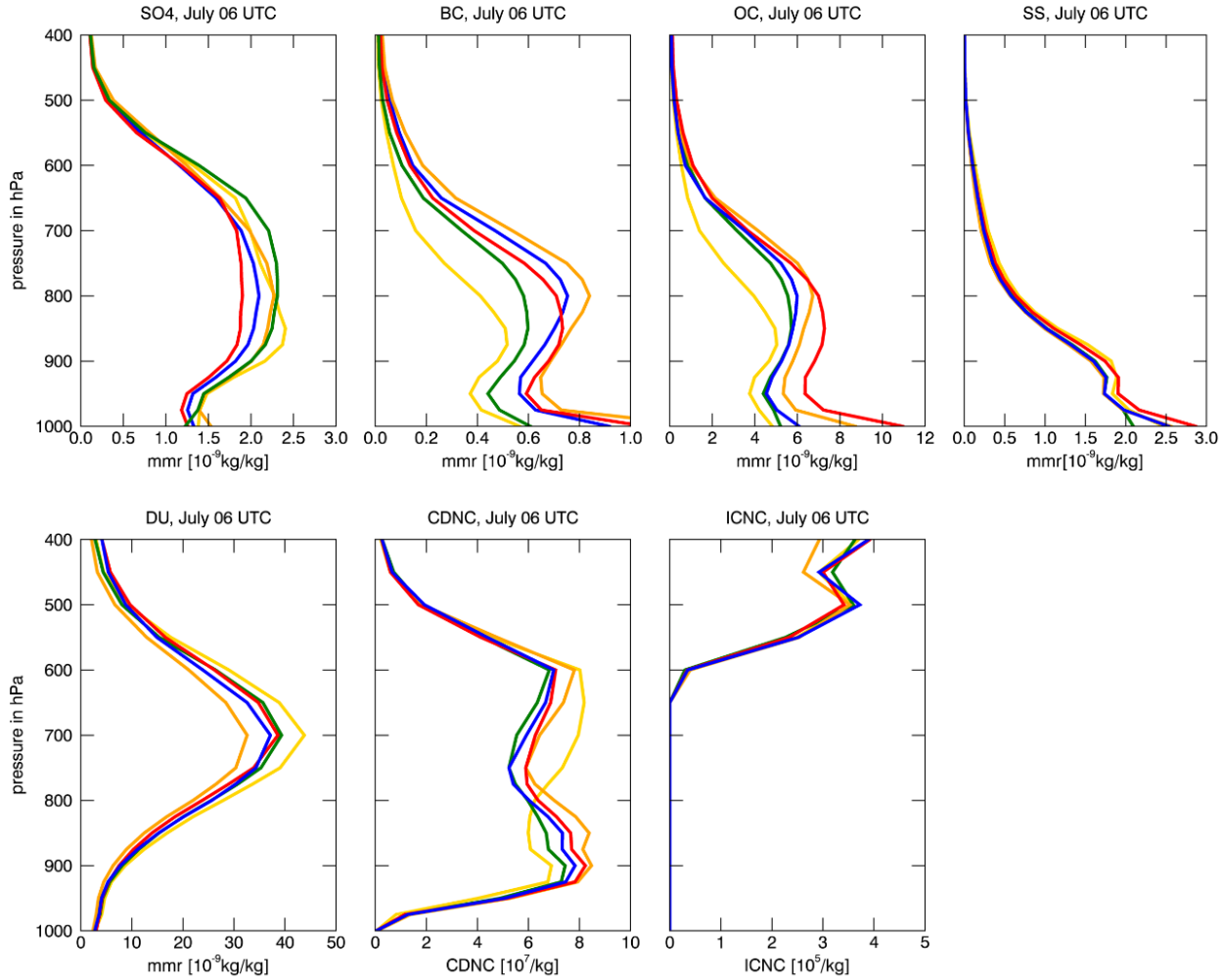

Figure 4.2: Simulated 10 year mean aerosol, cloud droplet number, and ice condensation nuclei concentration averaged over 8° W – 8° E, 5° N – 10° N for July, 06 UTC (gold – accmip, green – accmip_gfas, blue – htap, orange – ceds, red – dacciwa).

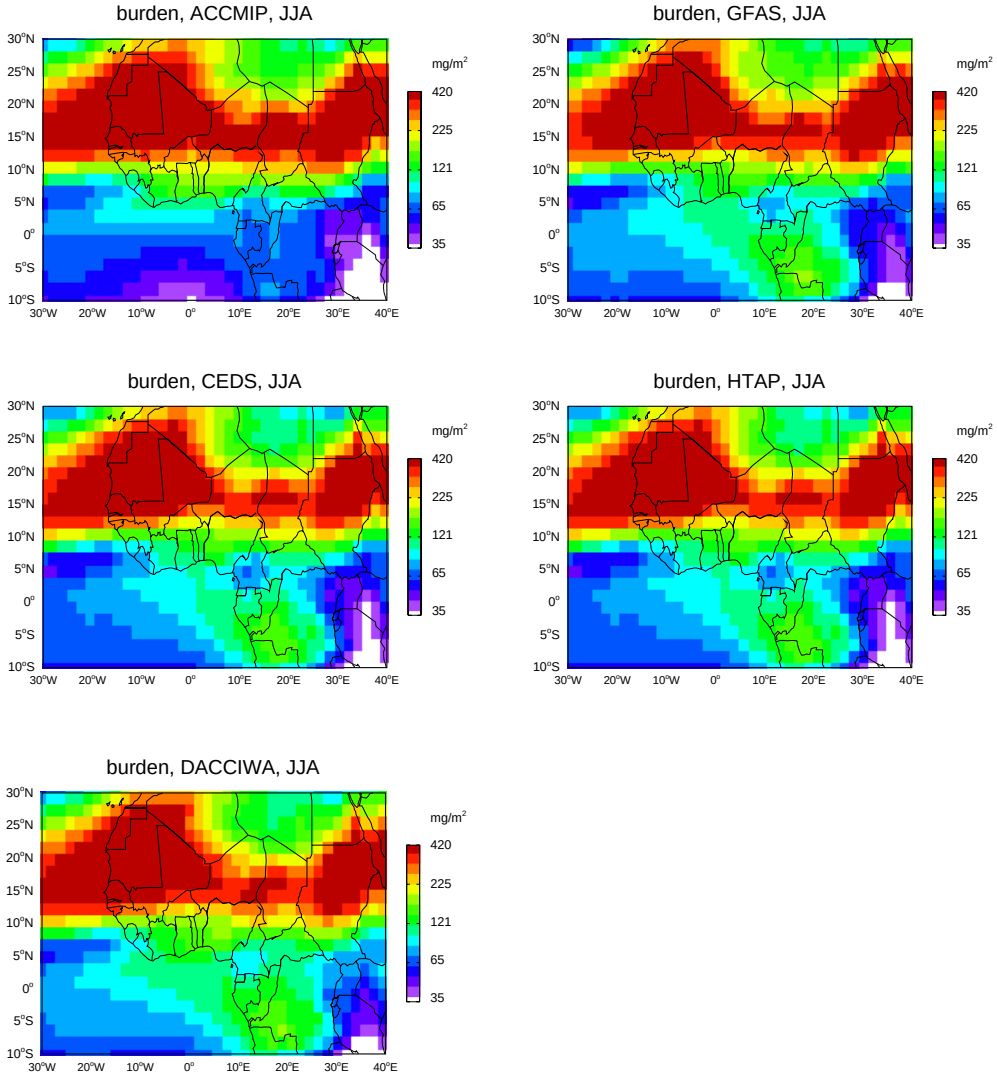

Figure 4.3: Long-term summer mean aerosol burden in West Africa as simulated by the different simulations with ECHAM6-HAM2 (respective simulation as indicated in the title).

4.3 Implications on simulated climate

Aerosols impact the climate via the direct and indirect aerosol effect. Although the aerosol distribution differs between the ECHAM6-HAM2 simulations, the 15-year averaged zonal mean (averaged between 10° W – 10° E) summer 2m temperature does not differ significantly between the simulations (figure 4.4). In comparison to different reanalysis data, the T 2m is overestimated by the simulations. This overestimation is more pronounced in the north than over the Guinea Coast itself. Therefore, the north – south temperature gradient is underestimated by the model.

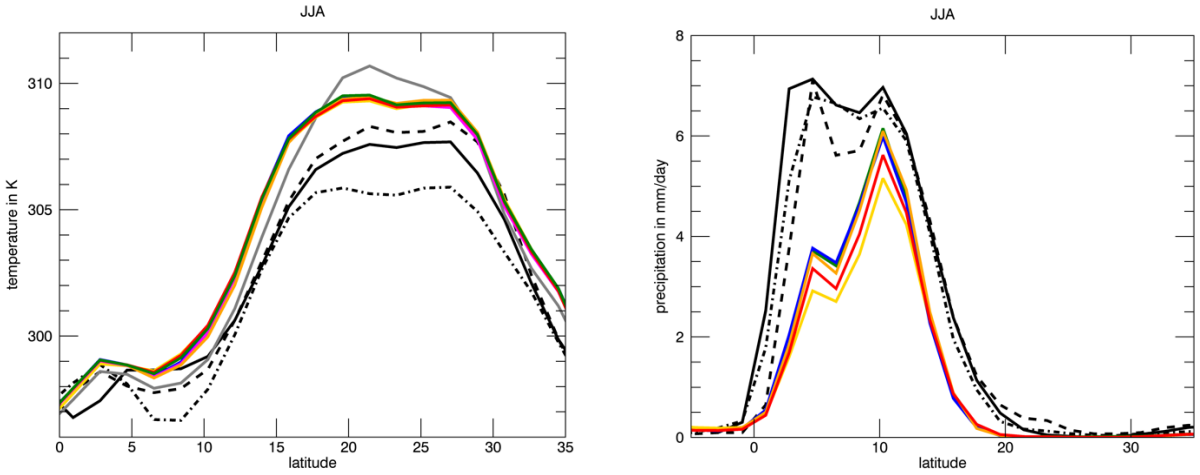

Figure 4.4: Long-term summer zonal mean (10° W – 10° E) 2 m temperature (left) and precipitation (right). Black lines indicate different reanalysis (solid: CRU; dashed: ERAinterim (T 2m), TRMM (precipitation); dashed-pointed: NCEP (T 2m), CMAP (precipitation)), grey lines correspond to an ECHAM6.3 simulation, and colored ones indicate the different ECHAM6-HAM2 simulations (yellow: accmip; green: accmip + gfas; orange: ceds; blue: htap, red: dacciwa).

In comparison to reanalysis, the 15-year zonal mean precipitation is underestimated by the model. The underestimation is more pronounced over the ocean (south of 5° N) than over the land. The overall location of the precipitation is captured reasonably by the model. The ECHAM6-HAM2 simulations differ between each other. The lowest precipitation flux is simulated by “accmip” (yellow line in figure 4.4) followed by “dacciwa” (red line). The aerosol concentration above 800 hPa is highest in simulation “accmip”, because the highest concentration of transported dust particles is simulated. Below 800 hPa the aerosol concentration is higher in simulation “dacciwa”, but it is even higher in “ceds” (orange line). Over ocean the aerosol burden is lowest in simulations “accmip” and strongest in “dacciwa” (figure 4.3). The results are consistent with the conclusions given in the last chapter: a high low-level cloud cover can reduce precipitation over the Guinea Coast. The results here show a similar effect for a high aerosol concentration in higher altitudes (around 800 – 600 hPa).

Aerosols as well as clouds impact the energy budget, which impacts the circulation. A prominent feature at the Guinea Coast during the West African monsoon season are nocturnal low-level clouds. They form shortly after sunset, spread during the night and dissipate in the late morning or early afternoon. The model does not resolve them adequately, the amount of low level clouds is underestimated and their diurnal cycle is not captured (figure 4.5). The mechanisms controlling the formation and maintenance of the low-level clouds were investigated by e.g. Schrage and Fink (2012), Schuster et al. (2013), and Adler et al. (2017). They are dominated by dynamical processes; the NLLJ and the monsoon flow bring cold air with enhanced relative humidity to the coast. On a smaller scale (few hundreds to a few tenth of kilometers) clouds are triggered by orographic induced lifting, gravity waves, and horizontal convergence upstream of existing clouds. Additionally, turbulent sub-grid-scale mixing is important for the upward shift of the clouds (Adler et al., 2017). These processes are not well captured by our as well as other climate models (Hannak et al., 2017; Deliverable 7.4). One reason is probably the rather coarse resolution of our model simulations, another could be convective parameterization (see chapter 3).

ECHAM6-HAM2 is one of the global climate models, which are somehow able to simulate the low-level clouds. But the cloud cover is underestimated and in particular, the diurnal cycle is not captured by the model. This behavior is already discussed in Deliverable 7.4.

The aerosol could impact the advection of cold air from the ocean due to modification in the temperature. The advection of cold air is essential for the development of low-level clouds. Since the south-north temperature gradient is reduced in our model simulations, less cold air is advected. This is one process which can explain the general underestimation in low-level cloud cover by the model simulations. To check if the reduction of cold air advection caused by the impact of aerosols on temperature is responsible for the differences in cloud cover between the simulations, the difference in T 2m between simulation “ceds” (highest low-level cloud cover, figure 4.5) and “accmip” (lowest low-level cloud cover) is shown in figure 4.6. Since the temperature is even warmer over the Gulf of Guinea in simulation “ceds” in comparison to simulation “accmip”, this process seems not to be responsible for the differences in cloud cover. One reason for the differences in cloud cover can be the different amount of cloud condensation nuclei (figure 4.2). But since aerosols, which act as cloud condensation nuclei, are usually present in our region of interest, the number of aerosols play a rather small part in the formation of the clouds. And the differences in cloud droplet number concentration (CDNC, figure 4.2) result in rather small changes in cloud cover (figure 4.5). In addition, changes in cloud cover can be explained by variations in humidity, stability, and variations in the strength of the low-level jet.

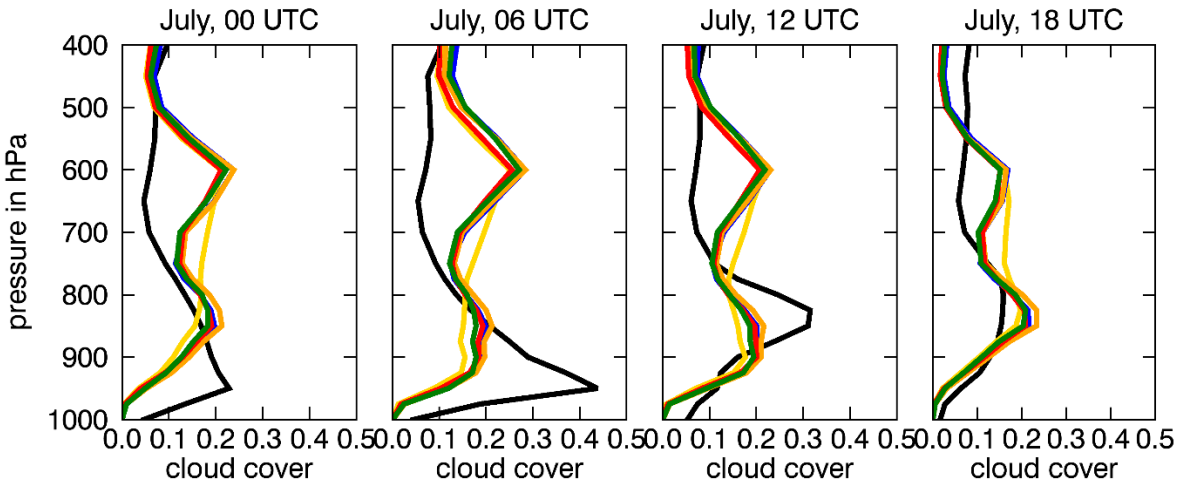

Figure 4.5: Simulated cloud cover averaged over 8° W – 8° E, 5° N – 10° N for July (avg. 1996-2010). The black line corresponds to ERAinterim reanalysis, colored lines show results of the different ECHAM6-HAM2 simulations (yellow – accmip, green – accmip_gfas, blue – htap, orange – ceds, red – dacciwa).

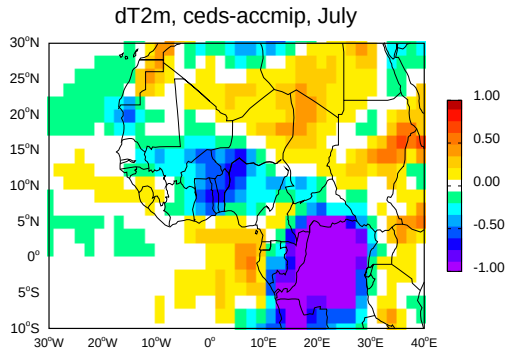

Figure 4.6: Difference in T 2m between ceds and accmip for July (multi monthly average).

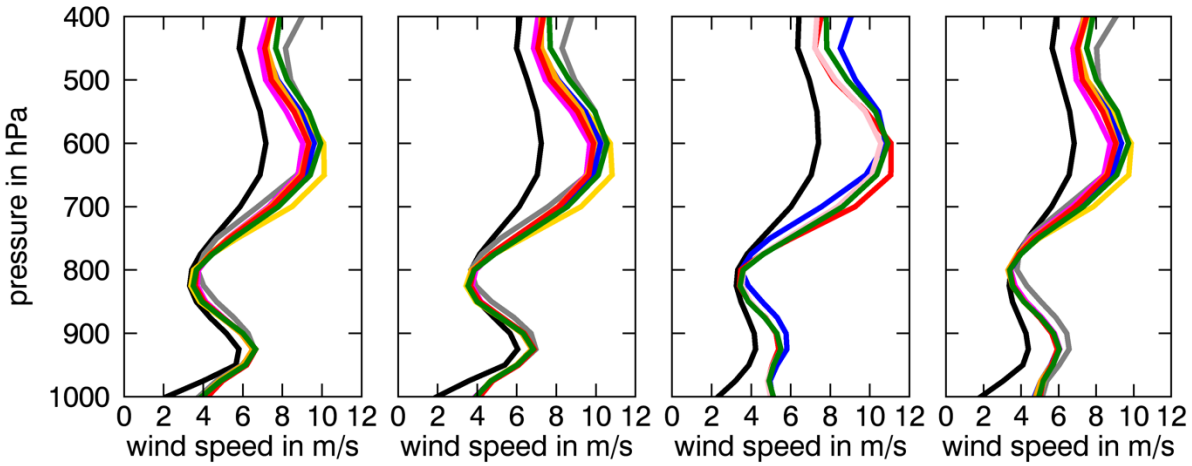

Figure 4.7: As figure 4.5, but for wind speed.

As discussed above, the dacciwa region is affected by the NLLJ during summer. The jet is captured by the model but the wind speed is overestimated and in particular, the diurnal cycle is not reproduced (figure 4.7). There is not a significant difference between the simulations in the representation of the NLLJ. The African Easterly Jet is another prominent feature in the West African Monsoon system. It is present at around 650 hPa. As discussed in Deliverable 7.4, ECHAM6-HAM2 simulates the African Easterly Jet too far south. Therefore, the wind speed is overestimated by the model at this altitude in the dacciwa box.

4.4 Summary and conclusions

ECHAM6-HAM2 as well as other global climate models have problems to capture the features of the West African monsoon system in an appropriate way (see also Deliverable 7.4). The near surface temperature is overestimated by the model. The amount of rainfall is largely underestimated over the Gulf of Guinea. The African Easterly Jet is simulated to far south. The low-level jet as well as the presence of low-level clouds are reproduced by the model, but the diurnal cycle is not existing in the model.

Estimates of emission fluxes show substantial differences between inventories in southern West Africa. This impacts the simulated distributions of anthropogenic as well as natural aerosols. The presence of aerosols modifies the regional energy budget via the direct and indirect aerosol effects. This has implications for the regional circulation. The emission flux of dust particles strongly depends on wind speed (emissions are proportional to the cubic of the wind speed). Changes in the circulation impact the emission, transport, and deposition of dust particles.

The differences in aerosol content do not impact the simulated climate significantly. The largest impact is seen on precipitation. Dynamical features like the African Easterly Jet, the NLLJ and connected to that the presence of low-level clouds are not impacted strongly by the differences in simulated aerosol content. Small changes in cloud cover are visible which could be caused by the differences in number of CDNC.

5 The role of sea surface temperature on projections of the West African Monsoon

We address the question how the climate could evolve in southern West Africa until the middle of this century. In general, climate projections rely on general circulation models, which cover a wide range of complexity. They range from atmosphere-only models to very complex Earth System Models (ESMs), which integrate the interactions of atmosphere, ocean, land, ice, and biosphere processes, they explicitly model the movement of carbon through the earth system. Aerosol-climate models account for interactions between anthropogenic and natural aerosol particles and the climate by altering the planetary energy balance through different mechanisms acting across a wide range of spatial scales: direct effects (Haywood and Boucher, 2000; Myhre, 2009), indirect effects (Lohmann and Feichter, 2005), and semi-direct effects (Hansen et al., 1997; Koch and Del Genio, 2010). They can be coupled to ESM-aerosol models (e.g. MPI-ESM-HAM2), but often aerosol models are coupled to atmosphere-only models. Here we present simulations with the aerosol-climate model ECHAM6-HAM2 as well to the ESM-aerosol model MPI-ESM-HAM2. We focus on the role of the SST for projections of the climate in southern West Africa.

5.1 Performed simulations

Dunning et al. (2017) show that CMIP5 simulations with coupled ocean-atmosphere models fail in representing the biannual precipitation regime over southern West Africa. This misrepresentation is related to a bias in the representation of the Intertropical Convergence Zone (ITCZ) (Richter and Xie, 2008; Roehrig et al., 2013; Toniazzo and Woolnough, 2014; Monerie et al., 2017). This bias is connected to the simulation of too warm Atlantic SSTs in the Gulf of Guinea (Vizy and Cook, 2001; Cook and Vizy, 2006; Roehrig et al., 2013), via influences on the meridional temperature gradient.

The misrepresentation of the eastern equatorial cold tongue during boreal summer could be associated with the restricted simulation of the northward progression of the ITCZ in global coupled atmosphere-climate models (Dunning et al., 2017; and references herein).

However, atmosphere only simulations with prescribed SST seem to reproduce the precipitation pattern in SWA better (Dunning et al., 2017). We are interested in the question how robust the projected changes of the West African climate are against the applied SST. Therefore, we decided to perform a set of simulations applying different SSTs to the ECHAM6-HAM2 model, and additionally, to compare these simulations with results of an MPI-ESM-HAM2 simulation (table 5.1). The atmospheric and aerosol component of the models are the same, but they do differ in the applied tuning.

For the AMIP based future projections, we apply the AMIP present day (1996-2016) SST distribution and add the estimated change in SST (mean(2040-2060) minus mean(1996-2016) of an ESM to it. Elguindi et al. (2014) evaluated ESM in terms of their capability to predict temperature and precipitation in different regions of the Earth (e.g. Africa). One goal of their study was to select ESM for forcing regional climate models. The selected model should be able to reproduce the present-day climate reasonable, capture a range of climate sensitivity and be somehow representative for the CMIP5 multi model mean. They found that MPI-ESM-MR, HadGEM2-ES and GFDL-ESM2M fulfil these goals. The HadGEM2-ES model simulates the highest response in temperature and precipitation to changes in forcing parameters. The ECHAM6 model is the atmospheric compound of the MPI-ESM (but ECHAM6.1). For these reasons we decided to use the output of both ESM CMIP5 simulations (each member 1) as basis for the SST.

To evaluate the role of the misrepresentation of the Atlantic SST pattern in ESMs on the projected change in climate we performed four additional simulations: We use the calculated SST of the Had-GEM-ES and MPI-ESM-MR (realization 1) for present day (PDcmip5H/M) and future (FUcmip5H/M_rcp8.5) conditions. Since the SST differs between the AMIP reanalysis and the ESM simulations, we had to re-tune the model to account for the energy conservation. For this purpose, the auto-conversion tuning parameter, which scales the conversion of cloud liquid water to rain in such a way that a balanced radiation budget at the top of the atmosphere is achieved, is reduced from 10.6 (default) to 7. The parameterization of Khairoutdino and Kogan (2000) is used in our model system.

We conducted simulations in T63 spectral resolution (approximately 200 km x 200 km) with ECHAM6.3-HAM2.3, based on the released version echam6.3.0-ham2.3. For simulating dust emission modifications of Stanelle et al. (2014) are included. The atmospheric column is subdivided into 47 vertical layers with a top at 0.1 hPa. The simulations differ in the applied representative concentration pathways (rcp) and/or the SST and sea ice cover, respectively. A summary of the simulations is given in table 5.1. For all ECHAM6-HAM2 simulations PD refers to an average over 1996-2014, and FU to 2040-2050.

The MPI-ESM-HAM2 simulation used in the current analyses spans the years from 2000 to 2054, initiated from a historical run and following the RCP8.5 scenario. The atmospheric component is run with a T63 horizontal grid (1.88° by 1.88°) and 47 hybrid vertical levels, while the ocean component uses the GR15L40 bipolar grid with poles situated over Greenland and Antarctica and 40 levels in the vertical (horizontal resolution of approximately 1.5°). Dynamical vegetation changes in response to climate change are considered (Brovkin et al., 2013). Changes between the present day and the future is examined by contrasting the ten-year mean centered around 2050 to the ten-year mean centered around 2010. The first five years of the simulation are not used to allow for model spin-up.

Table 5.1: Performed simulations

Simulation abbreviation	SST	Scenario
PDamip	AMIP	historical
PDcmip5H	HadGEM2	historical
PDcmip5M	MPI-ESM-MR	historical
FUamipH_rcp45	AMIP + dSST(HadGEM2)	rcp4.5
FUamipH_rcp85	AMIP + dSST(HadGEM2)	rcp8.5
FUamipM_rcp85	AMIP + dSST(MPI-ESM-MR)	rcp8.5
FUcmip5H_rcp85	HadGEM2	rcp8.5
FUcmip5M_rcp85	MPI-ESM-MR	rcp8.5
PD-ESM-HAM	Interactive, MPI-ESM-HAM2	historical
FU-ESM-HAM	Interactive, MPI-ESM-HAM2	rcp8.5

5.2 Sea surface temperature

The performed simulations differ amongst others in the applied SST. In figure 5.1 the long-term mean summer surface temperature of the different present day simulations is shown. The north-south temperature gradient between the hot Sahara in the north and the cold ocean in the south is more pronounced in the ECHAM6-HAM simulations, in particular in the amip based simulation. The warm bias at the Guinea Coast is visible in the cmip5 based simulations with ECHAM6-HAM2 and even more pronounced in the MPI-ESM-HAM2 simulation.

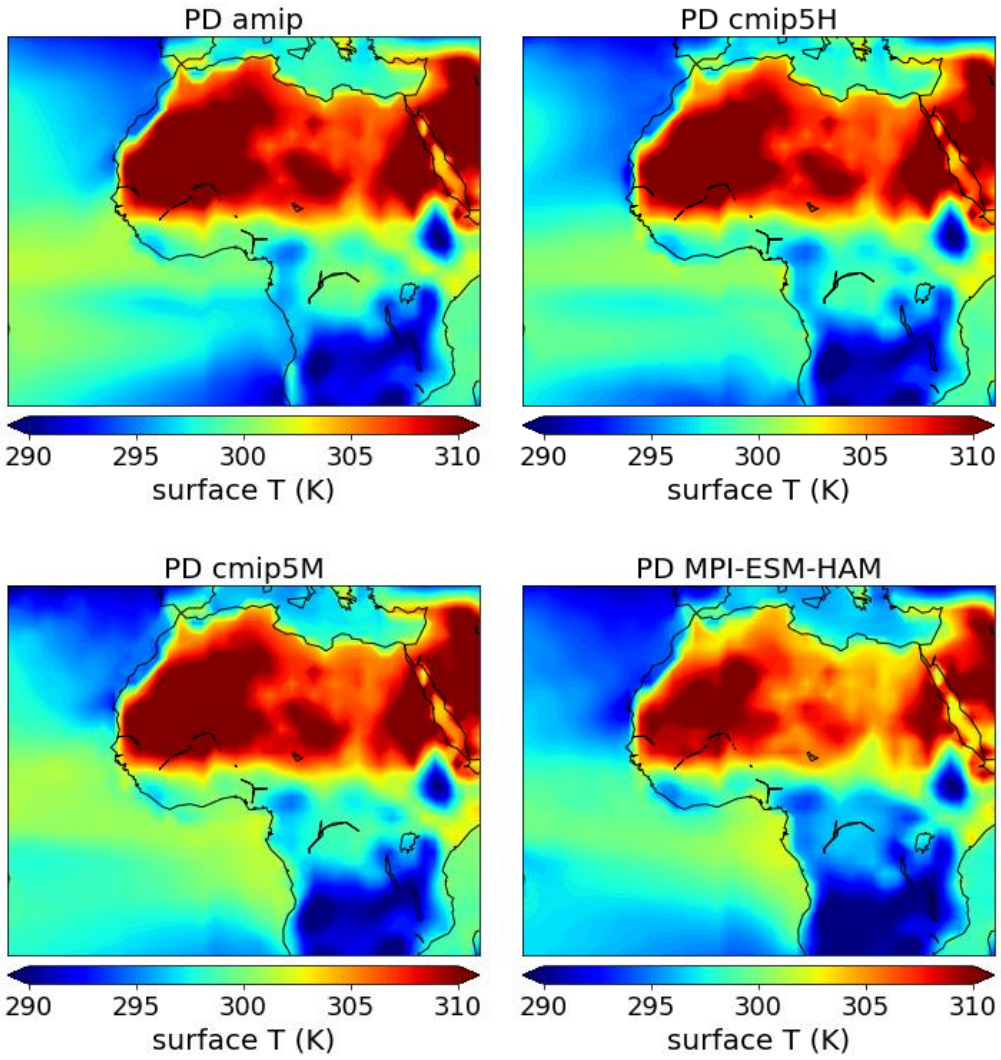

Figure 5.1: Long-term summer mean sea and land surface temperature as simulated by the different present day realisations.

In general, the projected change in summer surface temperature (over water equivalent to SST) is similar in the ECHAM6.3-HAM2.3 simulations (figure 5.2). In most of the places, over water as well as over land, an increase in temperature is expected. Over land, the warming is larger between 5° N and 10° N than further north. The strongest warming is calculated in the FUamipH_rcp8.5, and FUcmip5H_rcp8.5 scenarios, respectively. As expected, the lowest warming is simulated by FUamipH_rcp4.5. The pattern of the projected change in temperature given by the MPI-ESM-HAM2 simulation differs substantial from the ECHAM6-HAM2 simulations. Here, the strongest warming, around 4 K, is calculated to take place in the Sahara. The warming at the Guinea Coast is comparatively low with around 1 K.

All ECHAM6-HAM2 projections show a small decrease in surface temperature at the West Coast. This is caused by a change in vegetation cover. For present day conditions, the vegetation distribution estimated from satellite measurements is applied. But since the vegetation cover is expected to change in response to the applied scenario until the mid of the century, we applied a vegetation cover which is calculated in the MPI-ESM-MR for future conditions. Here, the natural vegetation cover is calculated in dependence of climatic variables (Brovkin et al., 2013). The dynamic vegetation model used in MPI-ESM-MR as well as in MPI-ESM-HAM2, simulates a rather high vegetation cover in the Sahara even for present day conditions. For the mid of the century, the vegetation cover is simulated to increase further, in particular the vegetation is expected to expand farther to the north. This feature will be discussed further in the next section and was already discussed in Deliverable 3.5. Since the model-based vegetation cover is calculated online, the change in vegetation cover between present day and future is smaller in the MPI-ESM-HAM simulations. Therefore, the expected decrease in temperature due to the increase of vegetation cover is smaller, and it can be compensated by the warming expected from higher trace gas concentrations. In the ECHAM6-HAM2 simulations the increase in vegetation cover is larger between present day and future, therefore the cooling of the surface is not fully compensated by the global warming.

Over water, all simulations project an increase in SST over the Gulf of Guinea. This increase is strongest if applying the rcp8.5 scenario and the HadGEM2 SST.

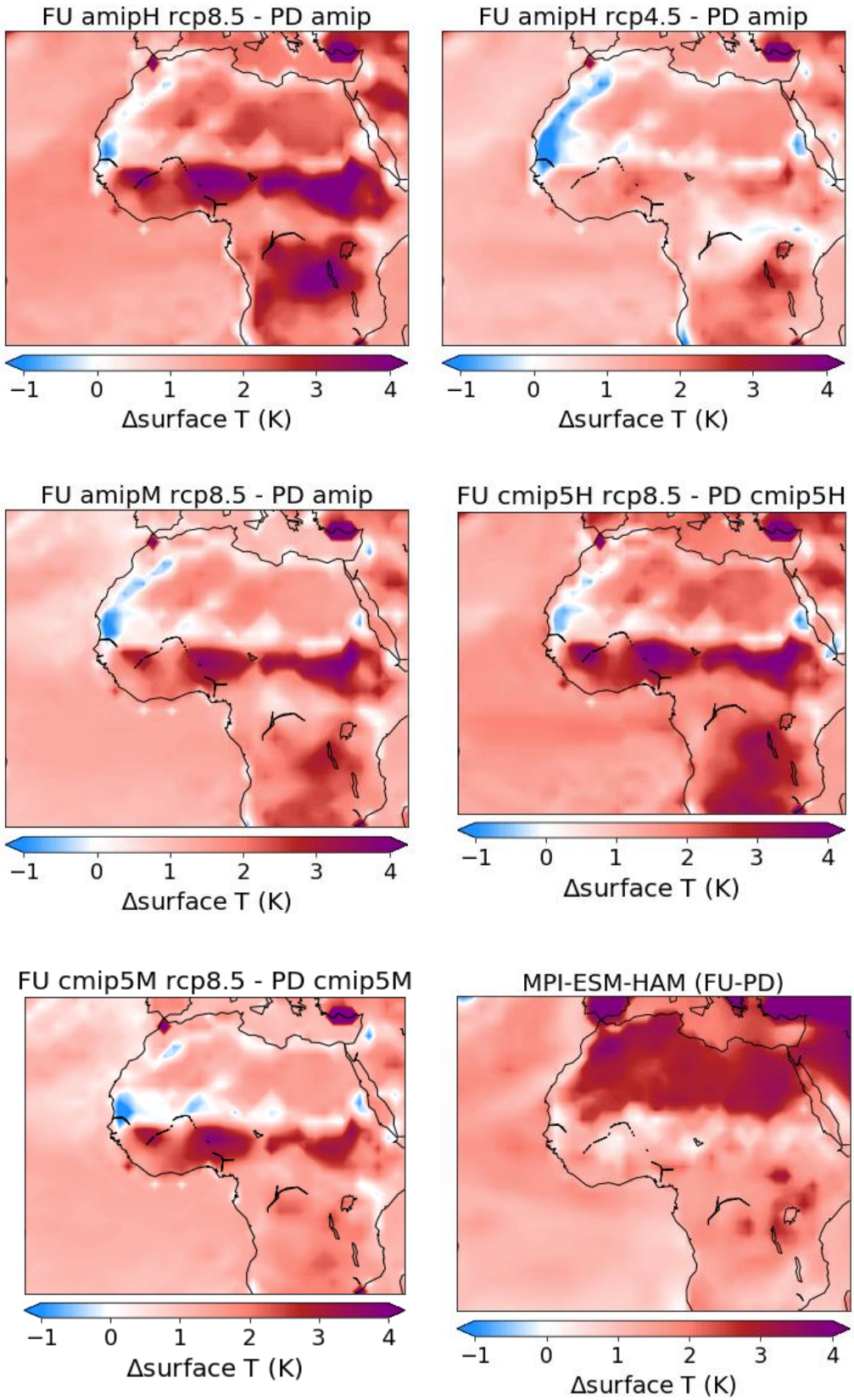

Figure 5.2: Projected future change in multi seasonal mean summer ocean and land surface temperature as simulated by the different model runs.

5.3 Tracer concentrations

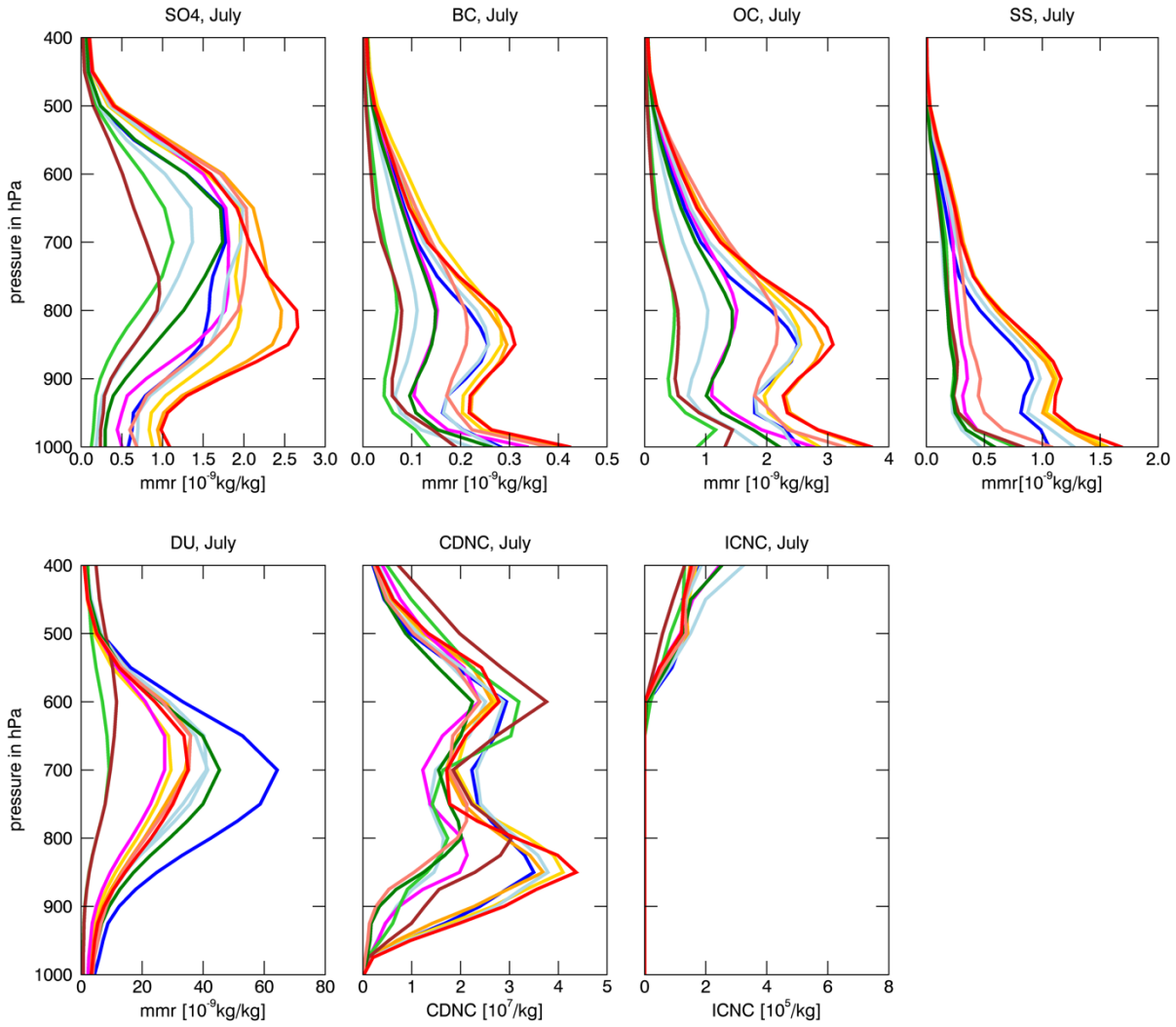

Figure 5.3: Multi-monthly mean vertical profile (averaged over DACCIWA box: 8° W – 8° E, 5° N – 10° N) of aerosol (SO4, black carbon, organic carbon, sea salt, dust), cloud droplet number, and ice condensation nuclei concentration for July. The colour coding is as follows: blue = PDamip, light blue = PDcmip5H, green = PDcmip5M, lime green = PD-ESM-HAM, gold = FUamipH_rcp45, red = FUamipH_rcp85, orange = FUamipM_rcp85, magenta = FUcmip5H_rcp85, salmon = FUcmip5M_rcp85, brown = FU-ESM-HAM).

The anthropogenic aerosol concentration as well as the sea salt concentration in southern West Africa is estimated to be lower in the MPI-ESM-HAM2 simulation in comparison to the ECHAM6-HAM2 simulations. This is caused mainly by a decrease in biomass burning aerosols, which are emitted in Central Africa and transported to the north. Since the MPI-ESM-HAM2 model simulated more precipitation over the ocean than ECHAM6-HAM2 (figure 5.4 and 5.5, will be discussed in the next section), the wet deposition of aerosols is higher. Therefore, less aerosols reach the coast.

Anthropogenic aerosol concentrations are expected to increase in future conditions. This is caused by an increase of anthropogenic aerosol emissions in West Africa. This increase is expected due to the expected increase in population and a further increase in industrialisation and urbanisation in that region. The increase in anthropogenic aerosol concentrations and the implication for human health are discussed in more detail in Deliverable 3.5.

Less dust particles are transported from the Sahara into our region of interest in the model simulations performed with the MPI-ESM-HAM (figure 5.3). This is caused by a higher vegetation cover in the Sahara, which is simulated by the dynamical vegetation model used in the MPI-ESM-HAM. This issue is already discussed and evaluated in Deliverable 3.5. The increase in vegetation cover results in an increase in roughness length, which then lowers the wind speed. Dust emissions are proportional to the cubic of the windspeed. Therefore, the dust emission flux is reduced.

All projections show a decrease in dust concentrations at the Guinea Coast until the mid of the century. The dust emission flux in the Sahara decreases (not shown). This is caused by the "Saharan greening" simulated by the MPI-ESM, which is discussed in Bathiany et al. (2014). Due to the CO_2 fertilization effect the vegetation cover is expected to increase in the Sahara until 2050. In all ECHAM6-HAM2 projections the vegetation cover was calculated by the MPI-ESM-MR CMIP5 simulations and fed to ECHAM6-HAM2, whereas the vegetation cover of the MPI-ESM-HAM2 simulation was calculated online. The MPI-ESM-HAM2 is based on a newer version of the MPI-ESM than the one used for the CMIP5 experiments. Here, the vegetation cover in the Sahara is estimated to be higher.

In the ECHAM6-HAM2 simulations, the increase in vegetation cover has a second impact on the dust emission flux. Dust particles can be only emitted in regions without or with low vegetation cover. Additionally, an increase in vegetation lowers the area where dust emissions can take place (availability of potential dust sources). These areas are derived online in our model simulations following the parameterization of Stanelle et al. (2014), where they are calculated in dependency of the model's vegetation cover. The decrease in potential dust sources results also in a decrease of dust emissions in the Sahara. If less dust is emitted, less particles are transported into the DACCIWA region.

The emission of sea salt particles depends, beyond others, on the water temperature, this is considered in the applied parameterization of Long et al. (2011). Since the SST is expected to increase in future conditions (figure 5.2) more sea salt particles are emitted and transported to the Guinea Coast.

5.4 Precipitation and near surface temperature

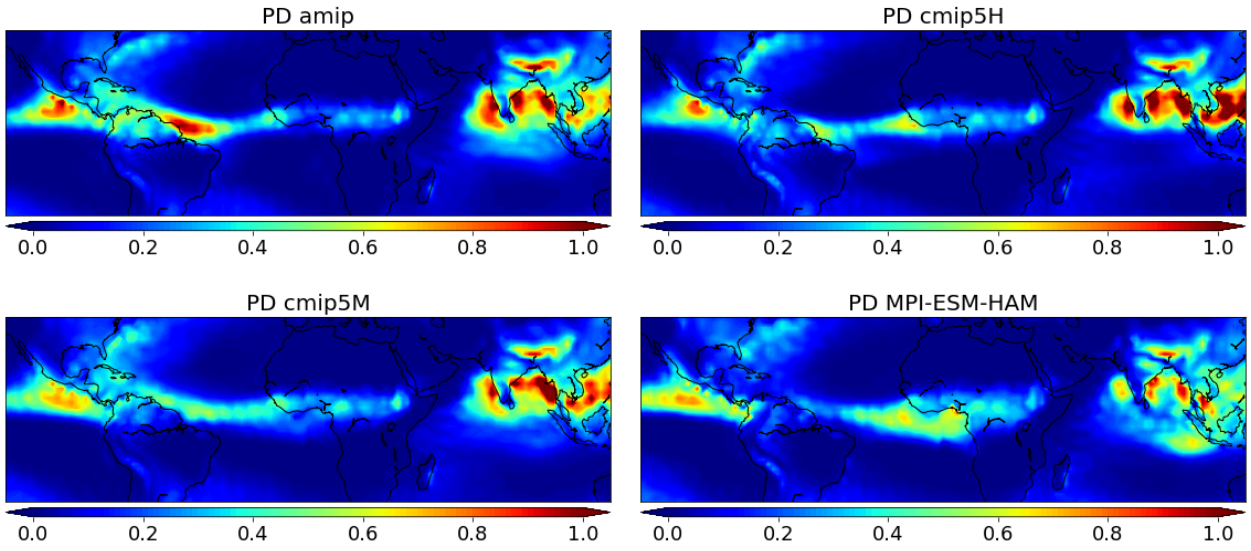

Figure 5.4: Long-term mean summer precipitation in mm/h as simulated by the different simulations for present day conditions.

The warm bias in SST over the eastern equatorial Atlantic is supposed to result in a misrepresentation of precipitation pattern in West Africa. The long-term mean summer precipitation

of the different present day simulations is shown in figure 5.4. The position of the rain band, which can be associated with the position of the Intertropical Convergence Zone (ITCZ), is in all simulations similar. But its southern extent over West Africa is stronger in the cmip5-based simulations as well as in the MPI-ESM-HAM2 simulation. The amount of precipitation over the Gulf of Guinea is highest in the MPI-ESM-HAM2. This is also visible when focusing on a zonal mean between 10° W – 10° E (figure 5.5, lime green line).

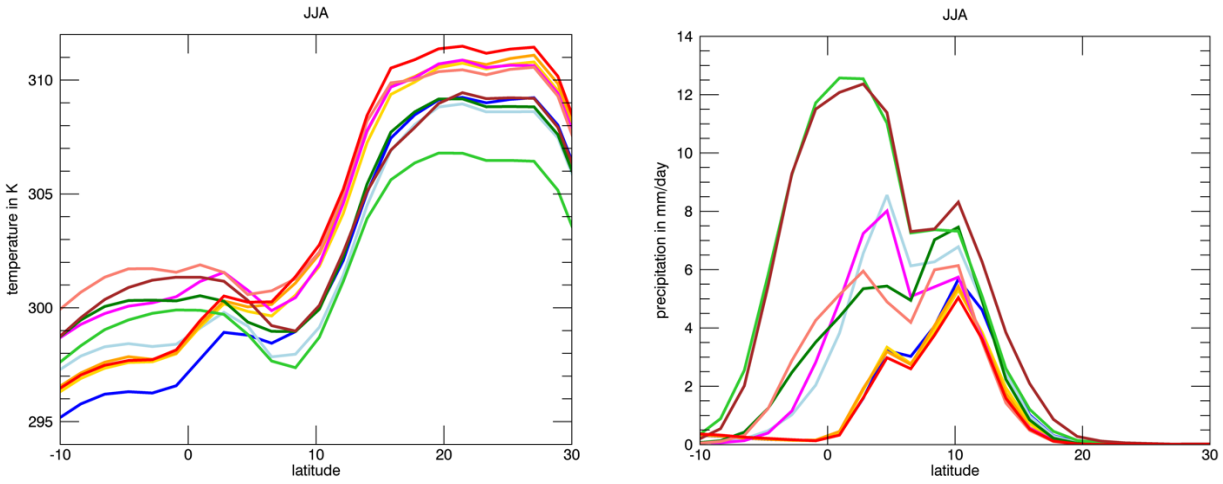

Figure 5.5: Long-term summer zonal (10° W – 10° E) mean 2 m temperature (left) and precipitation (right). The blueish/greenish colours correspond to present day simulations, the reddish ones to the future projections (colour code: blue = PDamip, light blue = PDcmip5H, green = PDcmip5M, lime green = PD-ESM-HAM2, gold = FUamipH_rcp45, red = FUamipH_rcp85, orange = FUamipM_rcp85, magenta = FUcmip5H_rcp85, salmon = FUcmip5M_rcp85, brown = FU-ESM-HAM2).

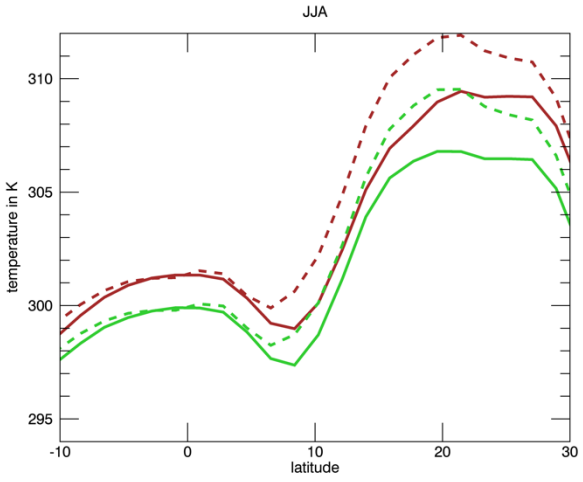

Figure 5.6: Long-term summer zonal (10° W – 10° E) mean 2 m temperature as simulated by the MPI-ESM-HAM2 (solid line) and the cmip5 simulation performed with the MPI-ESM-MR realization 1 (dashed lines) for present day conditions (green) and the mid of the century (brown).

The long-term mean summer 2 m temperature is highest over land in simulation MPI-ESM-HAM2. Also, when comparing the simulated SST of the MPI-ESM-HAM2 with the cmip5 experiment conducted with the MPI-ESM-MR (use of an older version of the same ESM but with prescribed aerosol distribution) the MPI-ESM-HAM2 SST is around 2.5 K lower (figure 5.6). Since the amount of dust particles emitted in the Sahara is rather low in the MPI-ESM-HAM2 simulation (see section 5.3) it is unlikely that the cooling of aerosols due to the direct aerosol effect causes this difference in temperature. The presence of vegetation is larger in the updated version of the MPI-ESM which is

coupled to the aerosol model. This results in a cooling of the surface and respectively of the T 2m. But also, the tuning between the MPI-ESM-HAM2 and the cmip5 version of the MPI-ESM differs. The differences in tuning are related to cloud properties (auto-conversion, entrainment, auto conversion for convective precipitation). We have tested the impact of the different tuning and the different vegetation distribution for present day between the ECHAM6-HAM2 model and the MPI-ESM-HAM2 on the simulated 2 m temperature in additional simulations (not shown here). Both factors are responsible for the large differences in T 2 m, but the tuning seems to be the dominant one. But also other so far unknown factors could contribute to the change in T 2 m.

All projections show an increase in 2 m temperature (figure 5.7). The ECHAM6-HAM2 simulation show the largest increase at 10° N. The increase varies between 2 (rcp4.5) and more than 3 K (rcp8.5). This is different in the MPI-ESM runs. Here the highest increase in temperature is simulated further north, in the Sahara. The increase is nearly 3 K. The changed pattern is caused by the differences in vegetation cover. As discussed above, the cooling induced by the Saharan greening is larger in the ECHAM6.3-HAM2.3 simulations, where we applied the satellite derived vegetation cover for present day. The warming induced by the increase in trace gas concentrations is compensated by the cooling due to changes in vegetation in the Sahara. This compensating effect is more pronounced in the simulations with ECHAM6.3-HAM2.3.

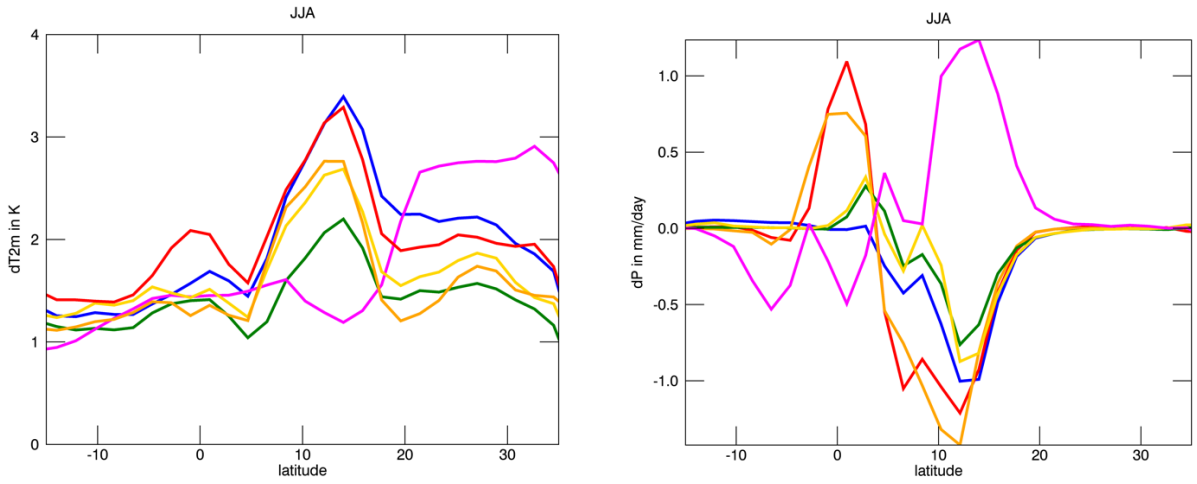

Figure 5.7: Projected change in multi seasonal summer zonal (10° W – 10° E) mean 2 m temperature (left) and precipitation (right). Colour coding: blue = FUamipH_rcp8.5 – PDamip, gold = FUamipM_rcp85 – PDamip, green = FUamipH_rcp45 – PDamip, red = FUcmip5H_rcp85 – PDcmip5H, orange = FUcmip5M_rcp85 – PDcmip5M, magenta = FU-ESM-HAM – PD-ESM-HAM.

All ECHAM6-HAM2 projections show, independent of the applied SST, a decrease in precipitation over land (figure 5.7 and 5.8). Only the strength of the decrease depends on the applied SST and scenario. The scenario simulating the highest low-level aerosol concentrations, FUamipH_rcp8.5, simulates the lowest precipitation flux. This again underlines the findings in chapter 3.

Over the ocean the signal is not as clear as over land. But there is a tendency that the precipitation will increase until the mid of the century. The cmip5 projection performed with the MPI-ESM-MR project a light decrease in precipitation over the Gulf of Guinea and an increase at the Guinea coast. This pattern is also simulated by MPI-ESM-HAM2, but the change is even more pronounced (figure 5.8). This differences in changing signal between MPI-ESM and ECHAM6-HAM2 simulation is striking when considering that the same SST is applied in MPI-ESM-MR and FUcmip5M_rcp85. Since the pattern is similar in MPI-ESM-MR and MPI-ESM-HAM2, the reason for the changing signal seems not to be caused by the HAM2 module. If we consider the simulations where we apply the

ESM derived vegetation cover in the present day simulations or where we applied nearly the same tuning in the ECHAM6-HAM2 simulation as it was used in the MPI-ESM-HAM2 simulation, nearly no change in precipitation is simulated over land. This could hint to the conclusion that the applied tuning and vegetation cover play a significant role for the projected change in precipitation. Overall, we can summarize that the changes in precipitation are very uncertain. The simulated change between present day and future is mostly smaller than the differences between the present day simulations itself. Therefore, results have to be taken with care. This corresponds with other studies (e.g. latest IPCC report).

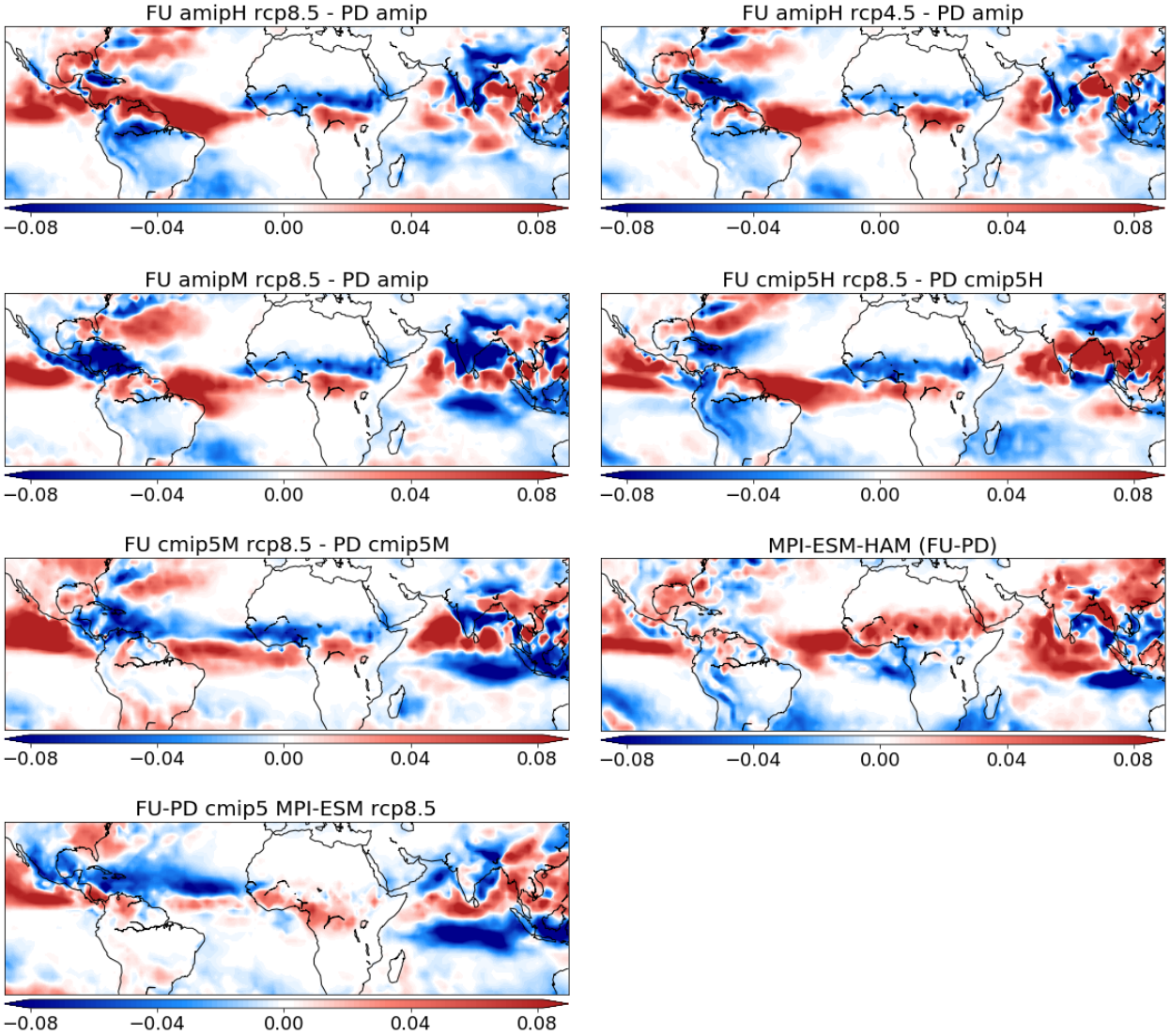

Figure 5.8: Change in long-term mean summer precipitation in mm/h between 2050 and present day as simulated by the different model realisations and by the cmip5 simulation member 1 with the MPI-ESM-MR (last row).

5.5 Low-level clouds

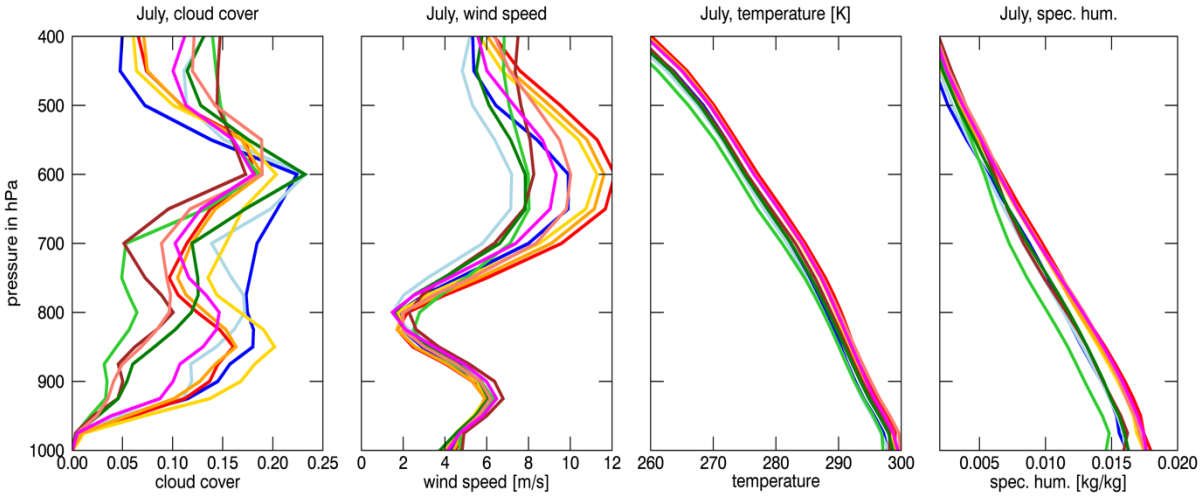

Figure 5.9: Multi monthly mean vertical profile of cloud cover, wind speed, temperature, and specific humidity averaged over 8° W – 8° E, 5° N – 10° N for July. Colour code: blue = PDamip, light blue = PDcmip5H, green = PDcmip5M, lime green = PD-ESM-HAM, gold = FUamipH_rcp45, red = FUamipH_rcp85, orange = FUamipM_rcp85, magenta = FUcmip5H_rcp85, salmon = FUcmip5M_rcp85, brown = FU-ESM-HAM.

In this section we focus on the presence of low-level clouds in our region of interest. As already discussed in chapters 3 and 4, low-level clouds are a prominent feature in southern West Africa. In general, ECHAM6.3 and ECHAM6.3-HAM2.3 are amongst the global climate models that are able to simulate them, but the strength and the daily cycle is underestimated (see Deliverable 7.4 and chapter 4). All rcp8.5 scenarios performed with ECHAM6-HAM2 show a decrease in cloud cover (figure 5.9). This is caused by an increase in SST. Therefore, the advection of cold air from the Gulf of Guinea to the Coast is reduced. The advection of cold air is essential for the development of low-level clouds (e.g. Adler et al., 2017). The increase in low-level cloud cover simulated by FUamipH_rcp4.5 could be caused by a lower increase in SST in comparison to the rcp8.5 scenarios (figure 5.5) and the increase in cloud droplet number concentration (CDNC, figure 5.3) due to the increase in anthropogenic emissions in 2050. The increase in CDNC cause an increase in cloud cover (see also chapter 4).

The low-level cloud cover over the DACCIWA region is smaller in the MPI-ESM-HAM simulations. But in contrast to the projections with ECHAM6-HAM2, MPI-ESM-HAM projections of the future cloud cover show an increase. In this projection, the largest warming is simulated in the Sahara, so north of the DACCIWA region. The specific humidity is supposed to increase. The cloud cover is a function of the relative humidity (RH), the decrease in RH due to the warming is over compensated by the increase in humidity. This results in an increase in low-level cloud cover.

6 Conclusions

Atmospheric models have difficulties to simulate the West African Monsoon system in an appropriate way. They show systematic errors when simulating e.g. precipitation and low-level clouds. These systematic errors were identified in Deliverable 7.4. In the current report we present sensitivity studies to analyse the impact of the radiative effects of low-level clouds on the West African Monsoon system and its diurnal cycle. The findings suggest that errors in the representation of low-level clouds can explain the large errors in the simulated precipitation at the Guinea Coastal region, but not in the Sahel.

The sensitivity study of low clouds mimics the effect of variations in aerosol concentration. An increase in aerosol content leads to more cloud condensation nuclei, they form more but smaller droplets. This increases the cloud optical thickness but can result in a reduction of the precipitation in the respective region (Twoomy effect). This effect is proved by simulations with the aerosol-climate model ECHAM6.3-HAM2.3. But in general, global models are parameterized to simulate a reduction in auto conversion when more aerosols are present. But large eddy simulations, which have usually a horizontal resolution of 25 – 100 m and a vertical grid spacing of 5 – 50 m, can produce the opposite effect when feedbacks are considered (e.g. Stevens et al., 2009).

Different anthropogenic aerosol inventories are applied to the model simulations. This impacts the regional energy budget and herewith the circulation. This feedbacks with the emission, transport, and deposition of natural aerosols (mainly dust). It is found that larger cloud droplet number concentrations (CDNC), which are linked to the aerosol concentrations, result in lower precipitation. This underlines the need of a realistic emission inventory for Africa to simulate the distribution of both anthropogenic and natural aerosols, as well as the climate in an appropriate way.

Although the formation of low-level clouds is a dynamical process, the presence of aerosols is needed. We show that the difference in aerosol concentrations and therefore of CDNC between the simulations result in small changes in low-level cloud cover. Dearden et al. (2018) conclude in their study, that, even for non-precipitating clouds, the evolution of low-level clouds is sensitive to the effects of droplet sedimentation. They argue that the sedimentation of droplets removes liquid water from the entrainment zone near the cloud top, this reduces the magnitude of evaporative cooling during the entrainment mixing. The growth rate of liquid water path increases during the night time and early morning. Ignoring the droplet sedimentation result in a reduction in the variability in liquid water path. They suggest that this mechanism should be included when performing large scale simulations for West Africa.

With parameterized convection, the model tends to have substantially more high and less low clouds compared with simulations with explicit convection. But both model realizations show difficulties in reproducing the observed state of the atmosphere. The impact of convection parameterizations on the West African meteorology is also documented in Marsham et al. (2013).

West Africa is one of the regions on Earth where anthropogenic aerosol emissions are expected to increase until the mid of the century. It is affected by the variability of the West African Monsoon rains. This makes the region vulnerable to climatic impacts related to health and food security (Knippertz et al., 2015). Therefore, it would be helpful to be able to predict the changes in climate in an appropriate way. Unfortunately, global climate as well as Earth System Models (ESM) are not able to reproduce the present day climate sufficient in this region. One important and well-known issue in Earth System Models is the warm bias in SSTs in the tropical Atlantic. Therefore, we present a broad set of future projections applying different SST in our aerosol climate model. Additionally, we discuss projections performed with an Earth System Model, which consists of the same atmospheric compound and is also coupled to the aerosol module.

The aerosol concentration depends on the applied emission inventory and scenario. But it also depends on the applied SST, vegetation cover and model system. The aerosol concentrations simulated in the MPI-ESM-HAM2 simulation are lower than in simulations with ECHAM6-HAM2. This is caused by differences in SST (lower SST results in lower sea salt emission flux), vegetation cover (higher vegetation cover in the Sahel/Saharan region results in decrease in dust emission flux) and increase in wet removal of aerosols caused by larger precipitation flux. But all projections result in the same conclusion, i.e. that the aerosol concentration is expected to increase during summer until the mid of the century. During winter the situation is more complicated, since the DACCIWA region

is mainly affected by dust particles which are transported from the Sahara into the region. The MPI-ESM-MR as well as the MPI-ESM-HAM project an increase in vegetation cover in the Sahara, the so-called Saharan greening, which is caused by the CO_2 fertilization effect (Bathiany et al., 2014). This causes a decrease in dust emissions and therefore less dust particles are transported to the south. The increase in anthropogenic aerosol concentrations can thus be compensated by the decrease in dust concentrations (see also Deliverable 3.5).

All performed projections show an increase in 2 m temperature until the middle of the century. Independent of the applied SST, all projections performed with ECHAM6.3-HAM2.3 simulate the largest increase at 10°N. In contrast, the MPI-ESM-HAM2 simulates the largest increase further north, i.e. in the Sahara.

There is no consensus in the projected change in precipitation between the model systems. All simulations performed with the aerosol climate model show a decrease in precipitation over land. Over ocean there is no agreement between the individual projections. The MPI-ESM-HAM simulations point to an increase in precipitation over land and a decrease over the ocean. This is in accordance with the cmip5 simulation performed with an older version of the MPI-ESM and without the coupled aerosol module. But the signal is more pronounced in the MPI-ESM-HAM simulation.

As discussed above low-level clouds can impact the amount of precipitation. If applying the rcp8.5 scenario, all ECHAM6-HAM2 simulations project a decrease in cloud cover caused by the increase in surface temperature. In contrast, the MPI-ESM-HAM simulates an increase in low-level cloud cover until the mid of the century. This is caused by the lower warming and an increase in humidity.

For West Africa, most of the results of the projections performed with ECHAM6-HAM2 and the MPI-ESM-HAM are in contrast to each other, although we applied the same SST in some projections. Therefore, we have to conclude that the projections of the West African climate are highly uncertain. One factor causing the uncertainty is the SST. We identified the differences in tuning factors of cloud parameters and the applied vegetation cover as reasons for the differences in the projected changes in climate between the aerosol climate model and the aerosol ESM when applying the same SST.

The differences in 2 m temperature and precipitation are larger between the present day simulations itself than the projected change until 2050. This points out the uncertainties in the representation of the African climate in the model. The gap in the observational network has to be filled in this part of the world to understand the WAM and to be able to represent it in an appropriate way in climate models.

7 References

Adler, B., Kalthoff, N., and Gantner, L., 2017: Nocturnal low-level clouds over southern West Africa analysed using high-resolution simulations, Atmos. Chem. Phys., 17, doi:10.5194/acp-17-899-2017.

Barker H. W., A. Marshak, W. Szymer, A. P. Trishchenko, J.-P. Blanchet, Z. Li, 2002: Inference of cloud optical depth from aircraft-based solar radiometric measurements. Journal of Atmospheric Sciences. 59, 2093-2111.

Bechtold P, Köhler M, Jung T, Doblas-Reyes F, Leutbecher M, Rodwell M, Vitart F, Balsamo G. 2008. Advances in simulating atmospheric variabilitywith the ECMWF model: From synoptic to decadal time-scales. Q. J. R. Meteorol. Soc. 134: 1337–1351.

Brovkin, V., Boysen, L., Raddatz, T., Gayler, V., Loew, A., and Claussen, M., 2013: Evaluation of vegetation cover and land-surface albedo in MPI-ESM CMIP5 simulations, Journal of Advances in Modeling Earth Systems, 5, 48–57, doi:10.1029/2012MS000169.

Dearden, C., Hill, A., Coe, H., and Choularton, T., 2018: The role of droplet sedimentation in the evolution of low level clouds over southern West Africa, Atmos. Chem. Phys. Discuss., https://doi.org/10.5194/acp-2018-269.

Deetz, K., Vogel, H., Knippertz, P.**,** Adler, B., Taylor, J., Coe, H., Bower, K., Haslett, S., Flynn, M., Dorsey, J., Crawford, I., Kottmeier, C., Vogel, B.: 2018: Numerical simulations of aerosol radiative effects and their impact on clouds and atmospheric dynamics over southern West Africa. *Atmos . Chem. Phys.*, 18, 9767–9788, doi:10.5194/acp-18-9767-2018.

Doms, G. and U. Schättler, 2004: A description of the nonhydrostatic regional model LM. Part II: Physical parameterization. Technical report, Deutscher Wetterdienst, Offenbach, (available from http://www.cosmomodel.org/public/documentation.htm).

Eltahir, E. A. B. and C. L. Gong, 1996: Dynamics of wet and dry years in West Africa. J. Climate, 9, 1030–1042.

Hannak, L., P. Knippertz, A.H. Fink, A. Kniffka, and G. Pante, 2017: Why Do Global Climate Models Struggle to Represent Low-Level Clouds in the West African Summer Monsoon?. J. Climate, 30, 1665–1687, https://doi.org/10.1175/JCLI-D-16-0451.1.

Heil, A., Kaiser, J. W., van der Werf, G. R., Wooster, M. J., Schultz, M. G., and Dernier van der Gon, H. , 2010: Assessment of the Real- Time Fire Emissions (GFASv0) by MACC, Tech. Memo, 628, ECMWF, Reading, UK.

Heise E, Ritter B, Schrodin E. 2006: 'Operational implementation of the multilayer soil model TERRA', Technical report. Deutscher Wetterdienst: Offenbach, Germany. http://www.cosmo-model.org.

Huang, W. T. K., Ickes, L., Tegen, I., Rinaldi, M., Ceburnis, D., and Lohmann, U., 2017: Global relevance of marine organic aerosol as ice nucleating particles, Atmospheric Chemistry and Physics Discussions, 1–34, doi:10.5194/acp-2017-922, 2017.

Hurley, J.V. and W.R. Boos, 2013: Interannual Variability of Monsoon Precipitation and Local Subcloud Equivalent Potential Temperature. J. Climate, 26, 9507–9527, https://doi.org/10.1175/JCLI-D-12-00229.1

Iacono, M. J., J. S. Delamere, E. J. Mlawer, M. W. Shephard, S. A. Clough, and W. D. Collins, 2008: Radiaitve forcing by long-lived greenhouse gases: Calculations with the AER radiative transfer models, J. Geophys. Res., 113, D13103, doi:10.1029/2008JD0099443.

Ickes, L., Welti, A., and Lohmann, U., 2017: Classical nucleation theory of immersion freezing: sensitivity of contact angle schemes to thermodynamic and kinetic parameters, Atmospheric Chemistry and Physics, 17, 1713–1739, doi:10.5194/acp-17-1713-2017.

Ilyina, T., Six, K. D., Segschneider, J., Maier-Reimer, E., Li, H., and Núñez-Riboni, I., 2013: Global ocean biogeochemistry model HAMOCC: Model architecture and performance as component of the MPI-Earth system model in different CMIP5 experimental realizations, Journal of Advances in Modeling Earth Systems, 5, 287–315, doi:10.1029/2012MS000178.

Jungclaus, J. H., Fischer, N., Haak, H., Lohmann, K., Marotzke, J., Matei, D., Mikolajewicz, U., Notz, D., and Storch, J. S., 2013: Characteristics of the ocean simulations in the Max Planck Institute Ocean Model (MPIOM) the ocean component of the MPI-Earth system model, Journal of Advances in Modeling Earth Systems, 5, 422–446, doi:10.1002/jame.20023.

Kaiser, J., and Coauthors, 2012: Biomass burning emissions estimated with a global fire assimilation system based on observed fire radiative power. Biogeosciences, 9 (1), 527.

Kaiser, J. W., A. Heil, M. O. Andreae, A. Benedetti, N. Chubarova, L. Jones, J.-J. Morcrette, M. Razinger, M. G. Schultz, M. Suttie, and G. R. van der Werf, 2012: Biomass burning emissions estimated with a global fire assimilation system based on observed fire radiative power, Biogeosciences, 9, 527-554, doi:10.5194/bg-9-527-2012.

Kalthoff, N., Lohou, F., Brooks, B., Jegede, G., Adler, B., Babic´, K., Dione, C., Ajao, A., Amekudzi, L. K., Aryee, J. N. A., Ayoola, M., Bessardon, G., Danuor, S. K., Handwerker, J., Kohler, M., Lothon, M., Pedruzo-Bagazgoitia, X., Smith, V., Sunmonu, L., Wieser, A., Fink, A. H., and Knippertz, P., 2018: An overview of the diurnal cycle of the atmospheric boundary layer during the West African monsoon season: results from the 2016 observational campaign, Atmos. Chem. Phys., 18, 2913-2928, https://doi.org/10.5194/acp-18-2913-2018.

Kniffka, A., Knippertz, P., and Fink, A. H., The role of low-level clouds in the West African monsoon system, Atmos. Chem. Phys. Discuss., subm.

Knippertz, P., A. H. Fink, R. Schuster, J. Trentmann, J. M. Schrage, and C. Yorke, 2011: Ultra-low clouds over the southern West African monsoon region, Geophys. Res. Lett., 38, L21808, doi:10.1029/2011GL049278.

P. Knippertz, H. Coe, J. C. Chiu, M. J. Evans, A. H. Fink, N. Kalthoff, C. Liousse, C. Mari, R. P. Allan, B. Brooks, S. Danour, C. Flamant, O. O. Jegede, F. Lohou, and J. H. Marsham, 2015: The DACCIWA project: Dynamics-aerosol-chemistry-cloud interactions in West Africa, B. Am. Meteorol. Soc., doi: http://dx.doi.org/10.1175/BAMS-D-14-00108.1.

Lamarque, J.-F., T. C. Bond, V. Eyrin, C. Granier, A. Heil, Z. Klimont, D. Lee, C. Liousse, A. Mieville, B. Owen, M. G. Schultz, D. Shindell, S. J. Smith, E. Stehfest, J. Van Aardenne, O. R. Cooper, M. Kainuma, N.Mahowald, J. R. McConnell, V. Naik, K. Riahi, and D. P. van Vuuren, 2010: Historical (1850-2000) gridded anthropogenic and biomass burning emissions of reactive gases and aerosols: methodology and application, Atmos. Chem. Phys., 10, 7017-7039, doi:10.5194/acp-10-7017-2010.

Lamarque, J.-F., and Coauthors, 2010: Historical (1850–2000) gridded anthropogenic and biomass burning emissions of reactive gases and aerosols: methodology and application. Atmospheric Chemistry and Physics, 10 (15), 7017–7039.

Leuenberger D, Koller M, Fuhrer O, Schär C. 2010: A generalization of the SLEVE vertical coordinate. Mon. Weather Rev. 138: 3683–3689.

Lin, S. J. and R. B. Rood, 1996: Multidimensional flux-form semi-Lagrangian transport schemes, Mon. Weather Rev., 124, 2046-2070.

Lohmann, U. and E. Roeckner, 1996: Design and performance of a new cloud microphysis scheme developed for the ECHAM general circulation model, Climate Dyn., 12, 557-572.

Lohmann, U. and Diehl, K., 2006: Sensitivity Studies of the Importance of Dust Ice Nuclei for the Indirect Aerosol Effect on Stratiform Mixed-Phase Clouds, Journal of the Atmospheric Sciences, 63, 968–982, doi:10.1175/JAS3662.1.

Lohmann, U., Stier, P., Hoose, C., Ferrachat, S., Kloster, S., Roeck- ner, E., and Zhang, J., 2007: Cloud microphysics and aerosol indirect effects in the global climate model ECHAM5-HAM, Atmos. Chem. Phys., 7, 3425–3446, doi:10.5194/acp-7-3425-2007.

Lott F, Miller M. 1997: A new subgrid-scale orographic drag parametrization: Its formulation and testing. Q. J. R. Meteorol. Soc. 123: 101–127.

Marsham, J. H., N. S. Dixon, L. Garcia-Carreras, G. M. S. Lister, D. J. Parker, P. Knippertz, and C. E. Birch, 2013: The role of moist con- vection in the West African monsoon system – in- sights from continental-scale convection-permitting simulations. Geophysical Research Letters, 40 (9), 1843–1849.

Marsland, S., Haak, H., Jungclaus, J., Latif, M., and Röske, F., 2003: The Max-Planck-Institute global ocean/sea ice model with orthogonal curvilinear coordinates, Ocean Modelling, 5, 91 – 127, doi:10.1016/S1463-5003(02)00015-X.

Mlawer, E.J., Taubman, S.J., Brown, P.D., Iacono, M.J., Clough, S.A. 1997: Radiative transfer for inhomogeneous atmospheres: RRTM, a validated correlated-k model for the longwave. J. Geophys. Res. 102: 16 663–16 682, doi:10.1029/97JD00237.

Raschendorfer M. 2001: The new turbulence parameterization of LM. COSMO Newsl. 1: 89–97. http://www.cosmo-model.org.

Roeckner, E., G.Baeuml, L. Bonventura, R. Brokopf, M. Esch, M. Giorgetta, S. Hagemann, I. Kirchner, L. Kornblueh, E. Manzini, U. Rhodin, U. Schlese, U. Schulzweida, A. Tomkins, 2003: The atmospheric general circulation model ECHAM5. Part I: Model description, Report 349, Max Planck Institute for Meteorology, Hamburg, Germany.

Schrage, J. M. and Fink, A. H.: Nocturnal continental low-level stratus over tropical West Africa, 2012: observations and possible mechanisms controlling its onset, Mon. Wea. Rev., 140, 1794–1809.

Schuster, R., Fink, A. H., and Knippertz, P., 2013: Formation and maintenance of nocturnal low-level stratus over the southern West African monsoon region during AMMA 2006, J. Atmos. Sci., 70, 2337–2355.

Seifert A. 2008: A revised cloud microphysical parameterization for COSMO–LME. COSMO Newsl. 8: 25–28. http://www.cosmo-model.org.

Stevens, B., G. Feingold, 2009: Untangling aerosol effects on clouds and precipitation in a buffered system, Nature, 461, 607-613.

Stevens, B., M. Giorgetta, M. Esch, T. Mauritsen, T. Crueger, S. Rast, M. Salzmann, H. Schmidt, J. Bader, K. Block, R. Brokopf, I. Fast, S. Kinne, L. Kornblueh, U. Lohmann, R: Pincus, T. Reichler, and E. Roeckner, 2013: Atmospheric component of the MPI-M Earth System Model: ECHAM6, James, 5, 146-172, doi:10.1002/jame.20015.

Stier, P., J. Feichter, S. Kinne, S. Kloster, E. Vignati, J. Wilson, L. Ganzeveld, I. Tegen, M. Werner, Y. Balkanski, M. Schulz, O. Boucher, A. Minikin, and A. Petzold, 2005: The aerosol-climate model ECHAM5-HAM, Atmos. Chem. Phys., 5, 1125-1156.

Sundqvist, H., E. Berge, and J. E. Kristjansson, 1989: Condensation and Cloud Parameterization studies with a mesoscale numerical weather prediction model, Mon. Weather Rev., 117, 1641-1657.

Vignati, E., J. Wilson, and P. Stier, 2004: An efficient size-resolved aerosol microphysics module for large-scale aerosol transport models, J. Geophys. Res., 109, D22202, doi:10.1029/2003JD004485.

Zängl, G., Reinert, D., Rípodas, P. and Baldauf, M., 2015: The ICON (ICOsahedral Non-hydrostatic) modelling framework of DWD and MPI-M: Description of the non-hydrostatic dynamical core. Q.J.R. Meteorol. Soc., 141, 563–579, doi:10.1002/qj.2378.

Zhang, K., D. O'Donnell, J. Kazil, P. Stier, S. Kinne, U. Lohmann, S. Ferrachat, B. Croft, J. Quaas, H. Wan, S. Rast, and J. Feichter, 2012: The global aerosol-climate model ECHAM-HAM, version 2: sensitivity to improvements in process representations, Atmos. Chem. Phys., 12, 8911-8949, doi:10.5194/acp-12-8911-2012.

Zheng, X. , Eltahir, E. A. and Emanuel, K. A.,1999: A mechanism relating tropical Atlantic spring sea surface temperature and west African rainfall. Q.J.R. Meteorol. Soc., 125: 1129-1163. doi:10.1002/qj.1999.49712555604.